

A quadrature-free Legendre polynomial approach for the fast modelling guided circumferential wave in anisotropic fractional order viscoelastic hollow cylinders

X. ZHANG¹), S. LIANG¹), S. SHAO²), J. YU¹)

¹) *School of Mechanical and Power Engineering, Henan Polytechnic University, 454003, Jiaozuo, P.R. China*

²) *School of Mathematics and Information Science, Henan Polytechnic University, 454003, Jiaozuo, P.R. China, e-mail: shuijunshao@163.com*

COMPARED TO THE TRADITIONAL INTEGER ORDER VISCOELASTIC MODEL, a fractional order derivative viscoelastic model is shown to be advantageous. The characteristics of guided circumferential waves in an anisotropic fractional order Kelvin–Voigt viscoelastic hollow cylinder are investigated by a quadrature-free Legendre polynomial approach combining the Weyl definition of fractional order derivatives. The presented approach can obtain dispersion solutions in a stable manner from an eigenvalue/eigenvector problem for the calculation of wavenumbers and displacement profiles of viscoelastic guided wave, which avoids a lot of numerical integration calculation in a traditional polynomial method and greatly improves the computational efficiency. Comparisons with the related studies are conducted to validate the correctness of the presented approach. The full three dimensional spectrum of an anisotropic fractional Kelvin–Voigt hollow cylinder is plotted. The influence of fractional order and material parameters on the phase velocity dispersion and attenuation curves of guided circumferential wave is discussed in detail. Moreover, the difference of the phase velocity dispersion and attenuation characteristics between the Kelvin–Voigt and hysteretic viscoelastic models is also illustrated. The presented approach along with the observed wave features should be particularly useful in non-destructive evaluations using waves in viscoelastic waveguides.

Key words: guided wave, fractional order derivative, anisotropic viscoelastic hollow cylinder, quadrature-free Legendre polynomial approach, dispersion, attenuation.

Copyright © 2021 by IPPT PAN, Warszawa

1. Introduction

IN RECENT YEARS, ULTRASONIC GUIDED WAVE HAS BEEN WIDELY USED in the non-destructive evaluation (NDE) of various structures, because it can provide a larger inspection range and the complete coverage of the waveguide cross-section compared with ultrasonic bulk waves [1, 2]. As an important step in the application of guided wave inspection techniques, accurate and highly efficient calculation of dispersive characteristics of guided waves and the associated displacement and stress profiles is extremely essential. Many appropriate theoretical

models are desired to study the characteristics of wave propagation in different waveguides such as the plate-like or pipe structures composed of isotropic or anisotropic, elastic or viscoelastic materials [3–5]. Viscoelastic materials, such as carbon fiber and epoxy resin, are widely used in integrated circuits, semiconductor devices, solar cells, and microelectromechanical systems, etc. [6]. The roots of attenuated modes caused by the viscoelasticity are important for NDE, but they are relatively difficult to obtain, especially for some complex cases involving anisotropy or curved waveguide structures. Hence reliable and effective methods to find all roots of the dispersion relation are very valuable.

The classical root-searching algorithm forms the basis of the DISPERSE software and it can solve various wave propagation problems [7, 8]. But it has some limitations, for instance, the material must be isotropic when dealing with cylindrical structures, and excluding the case involving generally anisotropic [9, 10]. Actually the introduction of curvature, viscoelasticity and anisotropic, can lead to expensive and tedious calculations. When considering the material viscoelasticity, the wavenumber is complex, and the search must be performed in \mathbb{C} for a given real frequency, a two dimensional space. This is a new challenge and algorithms to compute dispersion relations for waveguides are still under development. HOSTEN and CASTAINGS [11, 12] investigated the wave propagation in multilayered anisotropic media using the transfer matrix method, and pointed out the instabilities of the transfer matrix method for large frequency-thickness products. TORRES-ARREDONDO and FRITZEN [13] developed a higher order plate theory method to investigate the attenuation and phase velocity in an orthotropic viscoelastic plate, but this method failed to obtain precise results for higher order modes at high frequency. Using the Legendre polynomial approach, OTHMANI *et al.* [14], YU [15], SOUHAIL DAHMEN *et al.* [16] and HE *et al.* [17] investigated viscoelastic guided waves in layered and functionally graded waveguides. The polynomial approach suffers from the limitation of the time-consuming integral calculations and the difficulty in obtaining complete solutions of the transcendental dispersion equation. ZHU *et al.* [8] proposed a new root-searching algorithm to calculate the dispersion curves for anisotropic viscoelastic/elastic plates, and studied the attenuation jump and branches exchange in a viscoelastic model caused by conversion of wave mode shapes. Other common methods include the finite element method [18], the spectral collocation method [19, 20], the semi-analytical finite element method [21, 22]. Approaches to obtain dispersion relations usually reveal certain advantages and disadvantages in addressing some of these problems, so algorithms to compute dispersion relations for waveguides are still under development. The Legendre polynomial approach is very versatile in wave propagation problems, which can incorporate automatically boundary conditions into constitutive equations by a rectangular window function. Noted that in previous research work using the Legendre poly-

nomial approach, e.g. see [14–17], the dispersion relation is transformed into the solution of the vanishing determinant, namely $F(\omega, k) = 0$. Some root searching methods such as the Newton downhill method are used to solve it. These methods are iterative and very time consuming.

The Kelvin–Voigt model can be represented by a purely viscous damper and a purely elastic spring connected in parallel [23]. Stress σ , strain ε and their rates of change with respect to time t are governed by the equation

$$\sigma(t) = E\varepsilon t + \eta[d\varepsilon(t)/dt],$$

where E is a modulus of elasticity and η is viscosity. Studies have shown that traditional integer order viscoelastic models are limited in the accurate simulation of viscoelastic behavior, especially for the relationship between attenuation and viscosity. Compared to the integer order Kelvin–Voigt model, a fractional order viscoelastic model is shown to be advantageous since it requires fewer parameters to fit experimental data [24, 25]. Consequently, the time fractional Kelvin–Voigt model is proposed by the equation,

$$\sigma(t) = E\varepsilon(t) + \eta[d^\alpha\varepsilon(t)/dt^\alpha],$$

where α is the fractional order of the time differential [23,26]. When $\alpha = 1$, it becomes the traditional integer order Kelvin–Voigt model. The fractional order viscoelastic modeling begins with the idea from fractional calculus that the order of the derivative of the strain can be intermediate between 0 and 1 since it is the derivative of the strain that characterizes the material’s behavior. Moreover, the hollow cylinder, a common structure element, is widely used in many engineering applications. Investigations regarding the wave propagation characteristics in such a structure have been prosperous in recent decades, for instance, see [27–30]. However, the guided wave in an anisotropic fractional viscoelastic hollow cylinder, to the best of the authors’ knowledge, has not been studied before.

This study presents the quadrature-free Legendre polynomial approach combining the Weyl definition of fractional order derivatives for modeling dispersive solutions of guided circumferential waves in an anisotropic fractional Kelvin–Voigt viscoelastic hollow cylinder. The presented approach has an important advantage in computational efficiency compared to the existing polynomial approach, which can obtain dispersion solutions in a stable manner from an eigenvalue problem. It is easy to implement and non-iterative, and anisotropy is straightforwardly handled and all modes are easily obtained. The computational efficiency is assessed by the criterion of solving eigenvalues at given frequencies. The validity of the presented approach is verified by two examples. The full three dimensional (3D) spectrum of an anisotropic fractional Kelvin–Voigt

viscoelastic hollow cylinder is plotted. The influence of fractional order and material parameters (elastic modulus and viscoelastic modulus) on guided wave phase velocity dispersion curves and attenuation curves are discussed in detail. Moreover, dispersion solutions of both the integer order Kelvin–Voigt and hysteretic viscoelastic models are also illustrated to compare their differences. The traction-free boundary is assumed in this paper.

2. The description of the problem and the basic equations

2.1. The problem definition

Let us consider an anisotropic viscoelastic hollow cylinder with an infinite length in axial direction. A cylindrical coordinate system (r, θ, z) is applied to describe the cylinder geometry with an inner radius a and an outer radius b , as shown in Fig. 1. Coordinates r , θ and z are in the thickness, circumferential and axial directions. The thickness of the hollow cylinder is h ($h = b - a$), and the radius-thickness ratio $\eta = b/h$.

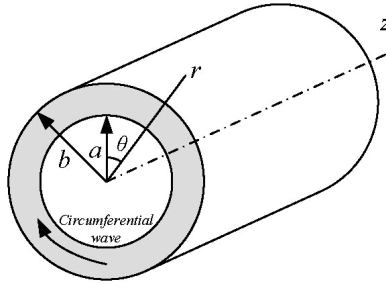


FIG. 1. Geometry of the problem.

The wave propagates along the circumferential direction with the wavenumber k and the angular frequency ω . The harmonic displacement, stress and strain field components are expressed by

$$(2.1) \quad \mathbf{u} = [u_r \ u_\theta \ u_z]^T, \quad \boldsymbol{\sigma} = [\sigma_r \ \sigma_\theta \ \sigma_z \ \sigma_{r\theta} \ \sigma_{rz} \ \sigma_{\theta z}]^T, \quad \boldsymbol{\varepsilon} = [\varepsilon_r \ \varepsilon_\theta \ \varepsilon_z \ \varepsilon_{r\theta} \ \varepsilon_{rz} \ \varepsilon_{\theta z}]^T.$$

Neglecting the body force, the equilibrium differential equations written in the cylindrical coordinate are,

$$(2.2) \quad \begin{cases} \partial_r \sigma_{rr} + \frac{1}{r} \partial_\theta \sigma_{r\theta} + \partial_z \sigma_{rz} + \frac{\sigma_{rr} - \sigma_{\theta\theta}}{r} = \rho \ddot{u}_r, \\ \partial_r \sigma_{r\theta} + \frac{1}{r} \partial_\theta \sigma_{\theta\theta} + \partial_z \sigma_{\theta z} + \frac{2}{r} \sigma_{r\theta} = \rho \ddot{u}_\theta, \\ \partial_r \sigma_{rz} + \frac{1}{r} \partial_\theta \sigma_{\theta z} + \partial_z \sigma_{zz} + \frac{1}{r} \sigma_{rz} = \rho \ddot{u}_z, \end{cases}$$

where $\partial_r = \partial/\partial r$, $\partial_\theta = \partial/\partial\theta$, $\partial_z = \partial/\partial z$, \ddot{u}_i ($i = r, \theta, z$) denote second-order derivatives with respect to time, and ρ is the material density.

The strain-displacement relations are given by:

$$(2.3) \quad \begin{aligned} \varepsilon_{rr} &= \partial_r u_r, \varepsilon_{\theta\theta} = \frac{1}{r} \partial_\theta u_\theta + \frac{u_r}{r}, & \varepsilon_{zz} &= \partial_z u_z, \\ \varepsilon_{r\theta} &= \frac{1}{2} \left(\partial_\theta u_r + \partial_r u_\theta - \frac{u_\theta}{r} \right), \\ \varepsilon_{rz} &= \frac{1}{2} (\partial_z u_r + \partial_r u_z), & \varepsilon_{\theta z} &= \frac{1}{2} \left(\partial_z u_\theta + \frac{1}{r} \partial_\theta u_z \right). \end{aligned}$$

For a generally anisotropic elastic material the constitutive relation can be expressed as

$$(2.4) \quad \boldsymbol{\sigma} = \bar{C}_{ijkl} \varepsilon_{kl} \pi(r), \quad i, j, k, l \in \{r, \theta, z\}$$

where $\pi(r)$ is a rectangular window function,

$$\pi(r) = \begin{cases} 1, & a \leq r \leq b, \\ 0, & \text{elsewhere,} \end{cases}$$

which is introduced to meet the stress-free boundary conditions, namely $\sigma_{rr} = \sigma_{r\theta} = \sigma_{rz}$ at $r = a$ and $r = b$. \bar{C}_{ijkl} is the material stiffness matrix and has 21 independent elements. For other materials, it has less independent components, e.g. the orthotropic material system with 9 independent elements. \bar{C}_{ijkl} in Eq. (2.4) can be defined to be complex quantities if the material is viscoelastic, namely $\bar{C}_{ijkl} = \tilde{C}_{ijkl} + i\mu_{ijkl}$, the real part represents the elastic moduli and the imaginary part its viscoelastic moduli [31]. Both the Kelvin–Voigt and hysteretic models are well established in ultrasonic nondestructive testing.

In the Kelvin–Voigt model [31], the complex component of the stiffness matrix C_{ijkl} is dependent on frequency, thus:

$$(2.5) \quad \bar{C}_{ijkl} = C_{ijkl} + i \frac{\omega}{\bar{\omega}} \mu_{ijkl} = C_{ijkl} + i \frac{f}{\bar{f}} \mu_{ijkl}.$$

The complex components of the stiffness matrix according to the hysteretic model [31] are independent of frequency, thus:

$$(2.6) \quad \bar{C}_{ijkl} = C_{ijkl} + i\mu_{ijkl},$$

where f is the frequency, \bar{f} is the characterization frequency and i is the imaginary unit. Obviously representation (2.6) for the hysteretic model could be regarded as a special case of (2.5) for the Kelvin–Voigt model when the frequency is equal to the characterization frequency.

For the fractional order Kelvin–Voigt viscoelastic model, the constitutive equation can be written as [23]:

$$(2.7) \quad \sigma_{ij} = C_{ijkl}\varepsilon_{kl} + \mu_{ijkl} \frac{\partial^\alpha \varepsilon_{kl}}{\partial t^\alpha},$$

where α is the order of the time derivative, $0 < \alpha \leq 1$. We use the Weyl definition of fractional order derivatives in this paper.

The α th order Weyl derivative of a function $f(t)$ is defined by [32, 33]

$$(2.8) \quad {}_t W_\infty^{-\alpha} f(t) = \frac{1}{\Gamma(\alpha)} \int_t^\infty (\tau - t)^{\alpha-1} f(\tau) d\tau$$

and for a harmonic function of $f(t) = e^{i\omega t}$, the Weyl fractional derivative has the property that $\partial^\alpha / \partial t^\alpha [e^{i\omega t}] = (i\omega)^\alpha e^{i\omega t}$.

Substituting Eqs. (2.3) and (2.5), (2.6) into (2.4)/(2.7) with following substitution into Eq. (2.2). As a result, three partial differential equations in terms of displacements are obtained. Eqs. (2.9), (2.10) and (2.11) are the resulting equations for an anisotropic fractional Kelvin–Voigt viscoelastic model, given in the Appendix. For the orthotropic case, Eqs. (2.9)–(2.11) are simplified to Eqs. (2.12)–(2.14). Obviously, Eq. (2.14) is decoupled and represents the circumferential SH wave Equations (2.12) and (2.13) are coupled and represent the circumferential Lamb-like wave.

2.2. Legendre orthogonal polynomial approach

For free harmonic waves propagating in the circumferential direction of a cylinder, the displacement components can be expressed

$$(2.15) \quad u_i(r, \theta, z, t) = \exp(ikb\theta - i\omega t)U_i(r)$$

where U_i ($i = r, \theta, z$) represent the displacement amplitudes in the three directions, respectively. Expanding them into the Legendre polynomial series as

$$(2.16) \quad U_i(r) = \sum_{m=0}^{\infty} p_m^i Q_m(r),$$

where p_m^i ($i = 1, 2, 3$) are the expansion coefficients,

$$Q_m(r) = \sqrt{\frac{2m+1}{(b-a)}} P_m\left(\frac{2r - (b+a)}{(b-a)}\right)$$

with P_m being the polynomial of the order m . The summation of polynomials in representation (2.16) can be truncated at a finite value M , when higher order terms do not cause any change in convergence.

Substituting representations (2.15) and (2.16) into (2.9), (2.10), (2.11), and multiplying both sides of the resulting Eqs. (2.9), (2.10) and (2.11) by n -order Legendre polynomials with n running from 0 to N , then integrating over r from a to b and making use of the orthonormality of the polynomials, yields:

$$(2.17) \quad k^2 \begin{bmatrix} A_{11}^{n,m} & A_{12}^{n,m} & A_{13}^{n,m} \\ A_{21}^{n,m} & A_{22}^{n,m} & A_{23}^{n,m} \\ A_{31}^{n,m} & A_{32}^{n,m} & A_{33}^{n,m} \end{bmatrix} \begin{Bmatrix} p_m^1 \\ p_m^2 \\ p_m^3 \end{Bmatrix} + k \begin{bmatrix} B_{11}^{n,m} & B_{12}^{n,m} & B_{13}^{n,m} \\ B_{21}^{n,m} & B_{22}^{n,m} & B_{23}^{n,m} \\ B_{31}^{n,m} & B_{32}^{n,m} & B_{33}^{n,m} \end{bmatrix} \begin{Bmatrix} p_m^1 \\ p_m^2 \\ p_m^3 \end{Bmatrix} \\ + \begin{bmatrix} C_{11}^{n,m} & C_{12}^{n,m} & C_{13}^{n,m} \\ C_{21}^{n,m} & C_{22}^{n,m} & C_{23}^{n,m} \\ C_{31}^{n,m} & C_{32}^{n,m} & C_{33}^{n,m} \end{bmatrix} \begin{Bmatrix} p_m^1 \\ p_m^2 \\ p_m^3 \end{Bmatrix} = -\omega^2 \begin{bmatrix} M_m^n & 0 & 0 \\ 0 & M_m^n & 0 \\ 0 & 0 & M_m^n \end{bmatrix} \begin{Bmatrix} p_m^1 \\ p_m^2 \\ p_m^3 \end{Bmatrix},$$

where M_m^n , $A_{j,l}^{n,m}$, $B_{j,l}^{n,m}$ and $C_{j,l}^{n,m}$ ($j, l = 1, 2, 3$) are the matrix elements and given in the Appendix; $j = 1$ refers to Eq. (2.12), $j = 2$ to Eq. (2.13), $j = 3$ to Eq. (2.14), $l = 1$ to p_m^1 or displacement u , $l = 2$ to p_m^2 or v and $l = 3$ to p_m^3 or w .

Or, more concisely,

$$(2.18) \quad k^2 \mathbf{A} \cdot \mathbf{P} + k^1 \mathbf{B} \cdot \mathbf{P} + \mathbf{C} \cdot \mathbf{P} = -\omega^2 \mathbf{M} \cdot \mathbf{P},$$

where \mathbf{A} , \mathbf{B} , \mathbf{C} , and \mathbf{M} are matrices of order $3(M + 1) \cdot 3(N + 1)$, and $\mathbf{P} = [p_m^1 \ p_m^2 \ p_m^3]^T$.

It is worth noting that in previous research work [14–17], by doing some mathematical manipulations, Eqs. (2.12)–(2.14) are expressed as the vanishing determinant of the coefficients of p . The vanishing determinant of this system is the dispersion relation. Some root-searching approaches such as the Newton downhill approach are used to solve it, which are iterative and very time consuming, especially for the big value M . To avoid the tedious iterative search procedure and improve the computational efficiency, here we present a quadrature-free Legendre polynomial approach, which can transform Eqs. (2.12)–(2.14) into a classical eigenvalue problem in the form $\mathbf{A}\mathbf{X} = \lambda\mathbf{X}$, instead of solving the vanishing determinant.

Obviously, Eq. (2.18) states a quadratic eigenvalue problem in k for a given real ω , and it does not have the structure of a general eigenvalue problem. Based on an algebraic manipulation known as the Linear Companion Matrix method [34], we recast Eq. (2.18) into a classical eigenvalue problem with the first-order wavenumber by doubling its algebraic size, as presented in the following.

Introducing a companion displacement vector field:

$$(2.19) \quad \mathbf{Q} = k \cdot \mathbf{P}.$$

Defining a companion matrix to (2.18) is

$$(2.20) \quad \mathbf{D} = \begin{bmatrix} \mathbf{0} & \mathbf{I}_{3(M+1)} \\ -\mathbf{A}^{-1}(\omega^2\mathbf{M} + \mathbf{C}) & -\mathbf{A}^{-1}\mathbf{B} \end{bmatrix},$$

where \mathbf{I} is the identity matrix.

Then Eq. (2.18) is more conveniently expressed as

$$(2.21) \quad \mathbf{D}\mathbf{X} = k\mathbf{X}$$

with $\mathbf{X} = [\mathbf{P} \ \mathbf{Q}]^T$.

It is a general eigenvalue problem in k , which can be solved by the ‘‘Eigenvalues’’ function in Mathematica. The real part of k ($\text{Re}(k)$) is related to the phase velocity by $Vp = \omega/\text{Re}(k)$, while the imaginary part of k ($\text{Im}(k)$) is a measure of attenuation. Moreover, eigenvectors represent the displacement or stress field distribution. In order to better process the solutions, we define the ratio $\lambda = \text{Re}(k)/\text{Im}(k)$. Once λ is given in a specified wavenumber range, all modes can be divided into two types. One is the propagating strongly attenuated mode, with a big $\text{Im}(k)$; the other is propagating lowly attenuated mode, with a small $\text{Im}(k)$. In some regions, k is almost purely imaginary and in figures this is indicated.

2.3. A quadrature-free polynomial approach with higher computation efficiency

Equation (2.17) involves various integral calculations, which were used to solve the dispersion relation in previous researches [14–17]. It is noteworthy that these integral calculations are very time-consuming, especially for the curved, damped and anisotropic media. To avoid calculating the time-consuming integral expressions, the analytic formulas of these integrals are derived by the recurrence relation and orthogonality of the Legendre polynomial. Equation (2.17) has the following five types of integral forms.

$$(2.22) \quad \begin{aligned} K_1 &= \int_a^b Q_n(r)Q_m(r) dr, & K_2 &= \int_a^b Q_n(r)\frac{d}{dr}Q_m(r) dr, \\ K_3 &= \int_a^b Q_n(r)\frac{d^2}{dr^2}Q_m(r) dr, & K_4 &= \int_a^b Q_n(r)Q_m(r)\frac{d}{dr}\pi(r) dr, \\ K_5 &= \int_a^b Q_n(r)\frac{d}{dr}Q_m(r)\frac{d}{dr}\pi(r) dr. \end{aligned}$$

Since the Legendre orthogonal polynomial is defined on a bounded interval $[-1, 1]$, we need to derive the analytical expressions of the above five integral

calculations for any interval $r \in [a, b]$. The derivation process is a little tedious and not given here. Using the integral transform technique and the properties of the Legendre polynomials, we can get.

For K_1 :

$$\begin{aligned}
 (2.23) \quad \int_a^b Q_m(r)Q_n(r) dr &= \sqrt{\frac{2m+1}{b-a}} \sqrt{\frac{2m+1}{b-a}} \\
 &\quad \times \int_a^b P_m\left(\frac{2r-(b+a)}{b-a}\right)P_n\left(\frac{2r-(b+a)}{b-a}\right) dr \\
 &= \frac{b-a}{2} \sqrt{\frac{2m+1}{b-a}} \sqrt{\frac{2m+1}{b-a}} \int_{-1}^1 P_m(t)P_n(t) dt \\
 &= \frac{b-a}{2} \sqrt{\frac{2m+1}{b-a}} \sqrt{\frac{2m+1}{b-a}} \frac{2}{2n+1} \delta(n, m)
 \end{aligned}$$

with

$$t = \frac{2r-(b+a)}{b-a}, \quad \delta(n, m) = \begin{cases} 1, & n = m, \\ 0, & n \neq m. \end{cases}$$

For K_2 :

$$\begin{aligned}
 \int_a^b rQ_m(r) \frac{d}{dz} Q_n(r) dr &= \sqrt{\frac{2m+1}{b-a}} \sqrt{\frac{2m+1}{b-a}} \\
 &\quad \times \int_a^b rP_m\left(\frac{2r-(b+a)}{b-a}\right) \frac{d}{dr} P_n\left(\frac{2r-(b+a)}{b-a}\right) dr \\
 &= \frac{b-a}{2} \sqrt{\frac{2m+1}{b-a}} \sqrt{\frac{2m+1}{b-a}} \int_{-1}^1 tP_m(t) \frac{d}{dt} P_n(t) dt \\
 &\quad + \frac{b+a}{2} \sqrt{\frac{2m+1}{b-a}} \sqrt{\frac{2m+1}{b-a}} \int_{-1}^1 P_m(t) \frac{d}{dt} P_n(t) dt.
 \end{aligned}$$

If $n + 1 > m$, and modulus $(n - m, 2) = 0$, $l = (n - m)/2$.

$$(2.24) \quad K_2 = \frac{b-a}{2} \sqrt{\frac{2m+1}{b-a}} \sqrt{\frac{2m+1}{b-a}} \frac{2(2n-4l+1)}{2m+1}.$$

And if $n = m$,

$$(2.25) \quad K_2 = \frac{b-a}{2} \sqrt{\frac{2m+1}{b-a}} \sqrt{\frac{2m+1}{b-a}} \frac{2(n+1)}{2n+1}.$$

And if $n > m$, modulus $(n-m, 2) = 1$, $l = (n-m-1)/2$.

$$(2.26) \quad K_2 = \frac{b+a}{2} \sqrt{\frac{2m+1}{b-a}} \sqrt{\frac{2m+1}{b-a}} \frac{2(2n-4l-1)}{2m+1}.$$

For K_3 :

$$(2.27) \quad \int_a^b r^2 Q_m(r) \frac{d^2}{dr^2} Q_n(r) dr = \frac{b-a}{2} \sqrt{\frac{2m+1}{b-a}} \sqrt{\frac{2m+1}{b-a}} \\ \times \int_{-1}^1 P_m(t) \left[\frac{d^2}{dt^2} P_n(t) - 2t \frac{d}{dt} P_n(t) + n(n+1) P_n(t) \right] dt \\ + (b+a) \sqrt{\frac{2m+1}{b-a}} \sqrt{\frac{2m+1}{b-a}} \int_{-1}^1 t P_m(t) \frac{d^2}{dt^2} P_n(t) dt \\ + \frac{(b+a)^2 b-a}{4} \frac{b-a}{2} \sqrt{\frac{2m+1}{b-a}} \sqrt{\frac{2m+1}{b-a}} \int_{-1}^1 P_m(t) \frac{d^2}{dt^2} P_n(t) dt \\ = \left[\frac{b-a}{2} + \frac{(b+a)^2 b-a}{4} \frac{b-a}{2} + (b+a) \right] \sqrt{\frac{2m+1}{b-a}} \sqrt{\frac{2m+1}{b-a}} \int_{-1}^1 P_m(t) \frac{d^2}{dt^2} P_n(t) dt \\ + [(n-1)(b+a) - (b-a)] \sqrt{\frac{2m+1}{b-a}} \sqrt{\frac{2m+1}{b-a}} \int_{-1}^1 P_m(t) \frac{d}{dt} P_n(t) dt \\ + \left[n(n+1) \frac{b-a}{2} - n(b-a) \right] \sqrt{\frac{2m+1}{b-a}} \sqrt{\frac{2m+1}{b-a}} \int_{-1}^1 P_m(t) P_n(t) dt$$

with

$$I_1 = \int_{-1}^1 P_m(t) P_n(t) dt = \frac{2}{2n+1} \delta(n, m);$$

and

$$I_2 = \int_{-1}^1 P_m(t) \frac{d}{dt} P_n(t) dt = \frac{2(2m-4l-1)}{2n+1},$$

here $m > n$, modulus $(m - n, 2) = 1$, $l = (m - n - 1)/2$. Otherwise, $I_2 = 0$.

And

$$I_3 = \int_{-1}^1 P_m(t) \frac{d^2}{dt^2} P_n(t) dt = \frac{2(2m - 4p - 3)(p + 1)(2m - 2p - 1)}{2n + 1},$$

here $p = \frac{m-n-2}{2}$, $k = \frac{m-n}{2}$, $m > n + 1$, modulus $(m - n, 2) = 0$. Otherwise, $I_3 = 0$.

For K_4 :

$$(2.28) \quad \int_a^b r Q_m(r) Q_n(r) \frac{d}{dr} \pi(r) dr = \int_a^b f(r) [\delta(r - a) - \delta(r - b)] dr = f(a) - f(b)$$

with $f(r) = r Q_m(r) Q_n(r)$.

For K_5 :

$$(2.29) \quad \int_a^b r^2 Q_m(r) \frac{d}{dz} Q_n(r) \frac{d}{dz} \pi(r) dr = \int_a^b g(r) [\delta(r - a) - \delta(r - b)] dr = g(a) - g(b)$$

with $g(r) = r^2 Q_m(r) \frac{d}{dz} Q_n(r)$.

The presented quadrature-free polynomial approach is very fast and easy to implement. The computational efficiency is discussed in the following section.

3. Implementation and verification of the quadrature-free polynomial approach

This section aims to validate the presented approach and discuss the calculation time of solving eigenvalues. Since guided wave in a fractional order waveguide has not been studied before, we firstly calculate the phase velocity dispersion and attenuation curves of a guided wave in the Kelvin-Voigt viscoelastic hollow cylinder ($\alpha = 1$) with big radius-thickness ratio ($a = 999$ mm, $\eta = 1000$), and make a comparison with the known results. The hollow cylinder with a sufficiently large radius-thickness ratio can be regarded as a flat plate.

Predictably, the dispersion curves of the hollow cylinder are the same as those of the plate with equivalent material. The material parameters are $\rho = 1560 \text{ kg/m}^3$, $C_{11} = 132 \text{ GPa}$, $C_{12} = 6.9 \text{ GPa}$, $C_{13} = 12.3 \text{ GPa}$, $C_{22} = 5.9 \text{ GPa}$, $C_{23} = 5.5 \text{ GPa}$, $C_{33} = 12.1 \text{ GPa}$, $C_{44} = 3.32 \text{ GPa}$, $C_{55} = 6.21 \text{ GPa}$, $C_{66} = 6.15 \text{ GPa}$, $\eta_{11} = 0.4 \text{ GPa}$, $\eta_{12} = 0.001 \text{ GPa}$, $\eta_{13} = 0.016 \text{ GPa}$, $\eta_{22} = 0.037 \text{ GPa}$, $\eta_{23} = 0.021 \text{ GPa}$, $\eta_{33} = 0.043 \text{ GPa}$, $\eta_{44} = 0.009 \text{ GPa}$, $\eta_{55} = 0.015 \text{ GPa}$, $\eta_{66} = 0.02 \text{ GPa}$, and $h = 1 \text{ mm}$, as given in references [1, 13]. The frequency of characterization is 2 MHz. The series expansions is $M = 20$.

Figure 2(a) shows the available results for the phase velocity dispersion curves from literature [13] based on a higher order plate theory. Figure 2(b) shows our results. We can easily notice that results of two above methods are in excellent agreement for the lower order modes. As pointed out in Reference [13, 14], the higher order plate theory suffers from some limitations that prevent it from being

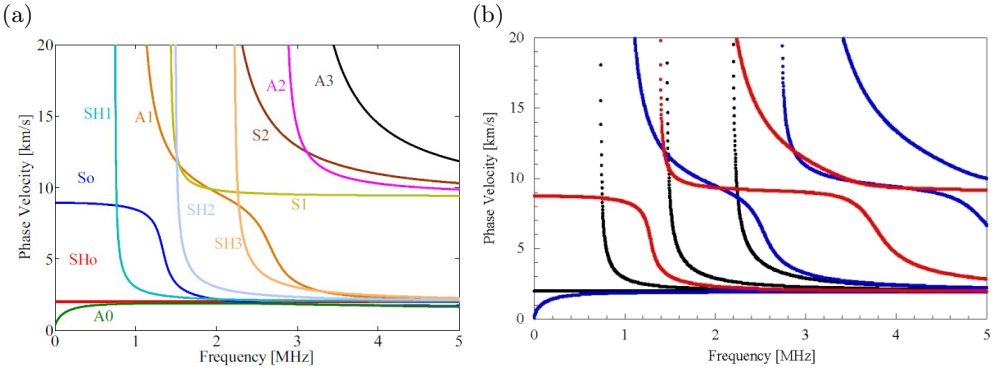


FIG. 2. Phase velocity dispersion curves: (a) the results from [13]; (b) our results, black-SH wave, red-symmetric Lamb wave, blue-antisymmetric Lamb wave.

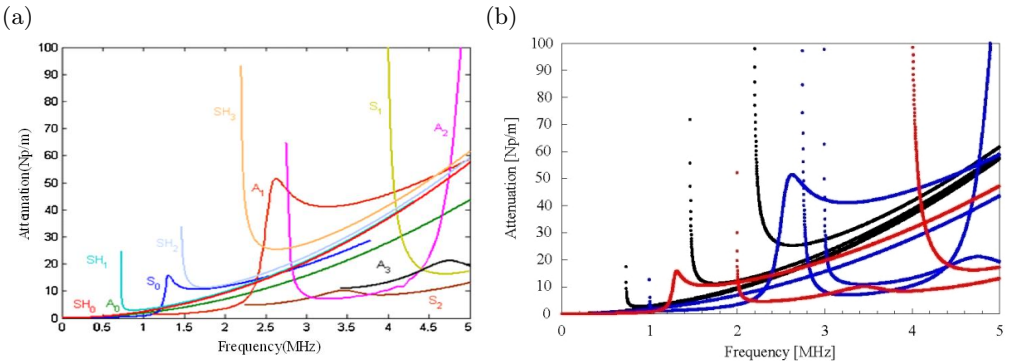


FIG. 3. Attenuation curves: (a) the results from [14]; (b) our results, with the same color scheme in Fig. 2(b).

used to solve the higher order modes in high frequency ranges. Figure 3(a) shows the attenuation curves from literature [14], and Fig. 3(b) shows our results. The attenuation curves obtained by our approach show good agreement with the known results, demonstrating the effectiveness of the presented approach.

Since the above example is an integer order Kelvin–Voigt model, we make a further validation on a fractional order Kelvin–Voigt viscoelastic hollow cylinder with small radius-thickness ratio. Equation (2.14) is decoupled and can be solved analytically. When the boundary condition is not considered, Eq. (2.14) becomes

$$(3.1) \quad r^2 \bar{C}_{44} W'' + r \bar{C}_{44} W' - k^2 b^2 \bar{C}_{66} W = -\rho r^2 \omega^2 W,$$

where W represents the displacement amplitude in the z directions.

The general solution of Eq. (3.1) is

$$(3.2) \quad W(r) = AJ[\lambda, \vartheta r] + BY[\lambda, \vartheta r],$$

where J and Y are Bessel functions of the first type and the second type, respectively, and A and B are undetermined coefficients, and

$$\lambda = \frac{\sqrt{k^2 b^2 \bar{C}_{66}}}{\sqrt{\bar{C}_{44}}}, \quad \vartheta = \frac{\sqrt{\rho} \omega}{\sqrt{\bar{C}_{44}}}.$$

Substituting Eq. (3.2) into the stress-free boundary condition, namely $T_{rz} = \bar{C}_{44} \frac{\partial u_z}{\partial r} = 0$, at $r = a$ and $r = b$, we have

$$(3.3) \quad \begin{vmatrix} J[\lambda - 1, \vartheta a] - J[\lambda + 1, \vartheta a] & Y[\lambda - 1, \vartheta a] - Y[\lambda + 1, \vartheta a] \\ J[\lambda - 1, \vartheta b] - J[\lambda + 1, \vartheta b] & Y[\lambda - 1, \vartheta b] - Y[\lambda + 1, \vartheta b] \end{vmatrix} = 0.$$

Therefore, Eq. (3.3) expresses the dispersion relationship of the circumferential SH wave.

We calculate the circumferential SH wave in the fractional Kelvin–Voigt viscoelastic hollow cylinder with $a = 9$ mm, $\eta = 10$ and $\alpha = 0.5$, and compare our results with the exact solutions, as shown in Fig. 4. We can see that polynomial results match very well the analytical ones.

The convergence of the Legendre polynomial approach was discussed in detail in previous research, and not evaluated again here. Having established the effectiveness of the presented approach, we now consider the computational cost. Since the process of solving eigenvalues takes the most of the computational time for obtaining phase velocity dispersion and attenuation curves, the efficiency of the polynomial approach is assessed by the criterion of solving eigenvalues at given frequencies. The integral calculation time, analytical formula calculation

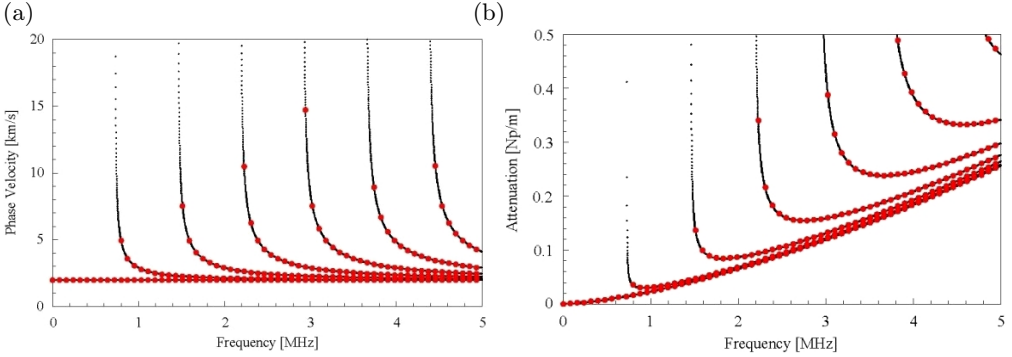


FIG. 4. Phase velocity and attenuation curves of the circumferential SH wave in a fractional viscoelastic hollow cylinder with $\alpha = 0.5$: (a) phase velocity curves; (b) attenuation curves.

time, total computational time for solving eigenvalues at 400 given input frequencies, and the proportion of the integral time and analytical calculation time to the total time are given (Desktop PC with Intel i5 CPU and 8 GB RAM). Tables 1 and 2 show a comparison in terms of these computational times taken to solve the eigenvalues for various truncation terms M . As can be seen from Table 1, the integral calculation takes up a majority of the total time, which occupies over 94% and reaches 357.196 s when $M = 30$. In comparison, the analytical calculation time is very short, less than 2s when $M = 30$, as shown in Table 2. The percentage of total time is small and decreases from 11.94% to 9.47% as M increases from 5 to 30. One can clearly see that the quadrature-free polynomial approach is less time consuming. The integral time decreases from

Table 1. The computation times of the existing polynomial approach with integral calculations.

t	M				
	5	10	15	20	30
Integral time	1.732	11.294	37.845	91.931	339.131
Total time	2.466	12.495	40.7	98.39	357.196
Percentage	70.24%	90.39%	92.99%	93.44%	94.94%

Table 2. The computation times of the quadrature-free polynomial approach.

t	M				
	5	10	15	20	* 30
Integral time	0.098	0.171	0.389	0.702	1.95
Total time	0.821	1.435	3.416	7.394	20.576
Percentage	11.94%	11.92%	11.39%	9.49%	9.47%

339.131 s to 1.95 s for $M = 30$, and the total time is reduced by several times or even several tens, e.g., 357.196 s compared with 20.576 s. This means a significant time saving when plotting a set of dispersion curves. Obviously the quadrature-free polynomial approach can dramatically improve the computational cost.

4. Numerical results and discussion

4.1. Guided circumferential waves in anisotropic viscoelastic hollow cylinders

4.1.1. Full three-dimensional (3D) spectrum A full 3D spectrum can provide a clearer visualization of the solutions and a better understanding of the nature of the modes, so we plot the 3D spectrum of the anisotropic Kelvin–Voigt viscoelastic hollow cylinder with $a = 9$ mm and $\eta = 10$, as shown in Fig. 5. The material parameters are taken from [20], and given as follows,

$$\begin{aligned}
 [\mathbf{C}] &= \begin{bmatrix} 74.29 & 28.94 & 5.86 & 0.20 & -0.11 & 37.19 \\ & 25.69 & 5.65 & 0.0928 & -0.0801 & 17.52 \\ & & 12.11 & 0.0133 & -0.0086 & 0.22 \\ & & & 4.18 & 1.31 & 0.0949 \\ \text{Sym} & & & & 5.35 & -0.0705 \\ & & & & & 28.29 \end{bmatrix} \text{ GPa,} \\
 [\eta] &= \begin{bmatrix} 218 & 76.5 & 16.4 & -3.60 & 0.688 & 116 \\ & 71.1 & 19.2 & -0.771 & 2.15 & 50 \\ & & 42.2 & -0.9644 & 0.627 & -3.07 \\ & & & 11.1 & 2.89 & -1.15 \\ \text{Sym} & & & & 13.6 & 1.48 \\ & & & & & 93.5 \end{bmatrix} \text{ MPa,}
 \end{aligned}$$

and $\rho = 1500 \text{ kg/m}^3$, $\bar{f} = 2 \text{ MHz}$. Figure 5 indicates that the spectrum exhibits a symmetry. One difference between the viscoelastic and elastic spectra concerns the symmetry. For the viscoelastic spectrum, all solutions are complex. Differently, the elastic spectrum has purely real, purely imaginary and complex branches, which is symmetric about the $k = 0$ and $\omega = 0$ planes. That is, for a given ω , if k is a solution, so is $-k$ and $\pm k^*$ (complex conjugate). But for the viscoelastic spectrum, this is only true at low frequencies. At high frequencies, if k satisfies the dispersion relation, then so do $-k$, but not their complex conjugates. The viscoelastic spectrum exhibits the central symmetry. Therefore the full 3D spectrum can be characterized by only the positive $\text{Im}(k)$ versus ω . And rotating them by 180° around the ω axis, the negative imaginary part can be obtained. We can find that each minimum and maximum of the segments of the almost purely imaginary branches is a point of intersection with a complex branch. To the best of the authors' knowledge, the full 3D spectrum for an

anisotropic Kelvin–Voigt viscoelastic hollow cylinder presented here has not been published before. Furthermore, we calculate the 2D phase velocity dispersion and attenuation curves of a viscoelastic hollow cylinder with big radius-thickness ratio ($\eta = 1000$, $a = 999$ mm), approximately regarded as a plate. The obtained results are shown in Fig. 6. Its good agreement with the available results of a plate in [20] from the semi-analytical finite element method was checked by authors, and no difference was found between them. This once again shows the

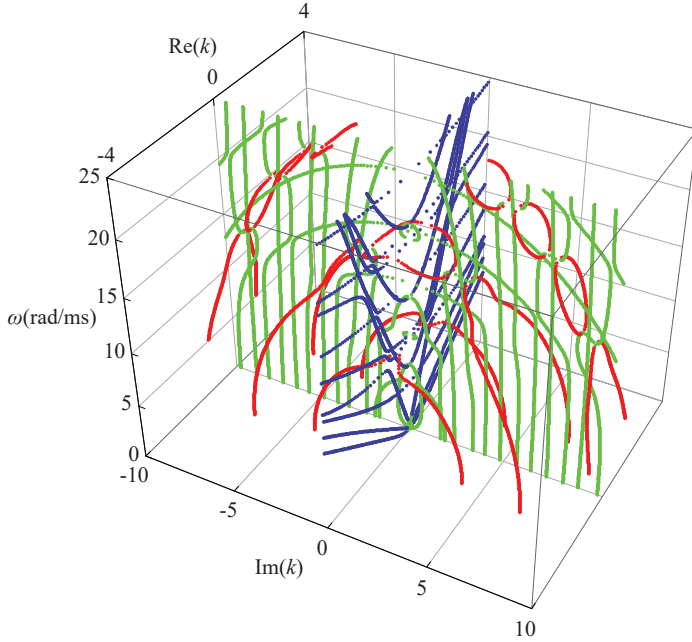


FIG. 5. Full 3D spectrum of an anisotropic Kelvin–Voigt viscoelastic hollow cylinder.

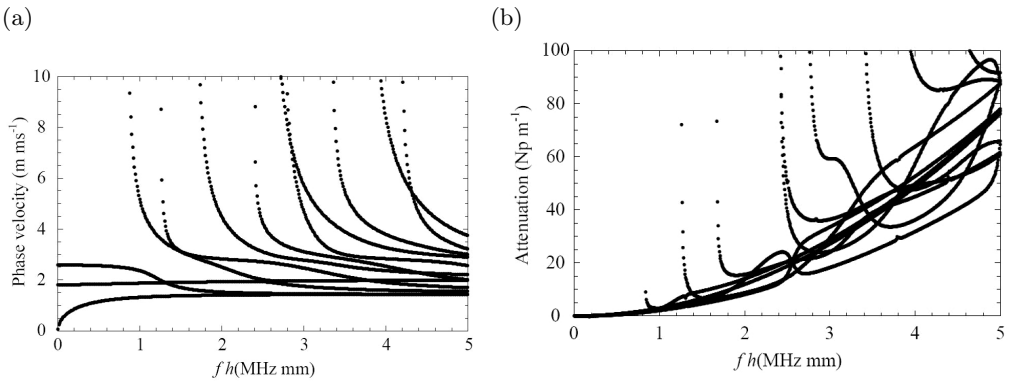


FIG. 6. (a) Phase velocity dispersion and (b) attenuation for a viscoelastic hollow cylinder with a large radius-thickness ratio.

validation of our approach. The literature results can be found in [20] and are not reproduced here.

4.1.2. Comparisons of two viscoelastic models. In this section, the guided wave characteristics of both the Kelvin–Voigt and the hysteretic viscoelastic models are respectively illustrated to compare their differences. Figure 7 presents the resulting phase velocity dispersion and attenuate curves for the two viscoelastic hollow cylinder models, with $a = 9$ mm and $\eta = 10$. We can clearly see from Fig. 7(a) and Fig. 7(b) that both models do not affect the phase velocity dispersion results in a substantial manner. But significant effects can be found on the attenuation curves illustrated by Fig. 7(c) and 7(d). The attenuation of the low order modes increases linearly with frequency in the hysteretic model, but increases by a quadratic function of the frequency in the Kelvin–Voigt model. At the characterization frequency 2 MHz, the attenuations of the two models are the same. This is because both models have an equivalent material stiffness matrix at this frequency. For the Kelvin–Voigt model, the attenuation is smaller when the working frequency $f < \bar{f}$, and larger when $f > \bar{f}$, compared with the hysteretic model.

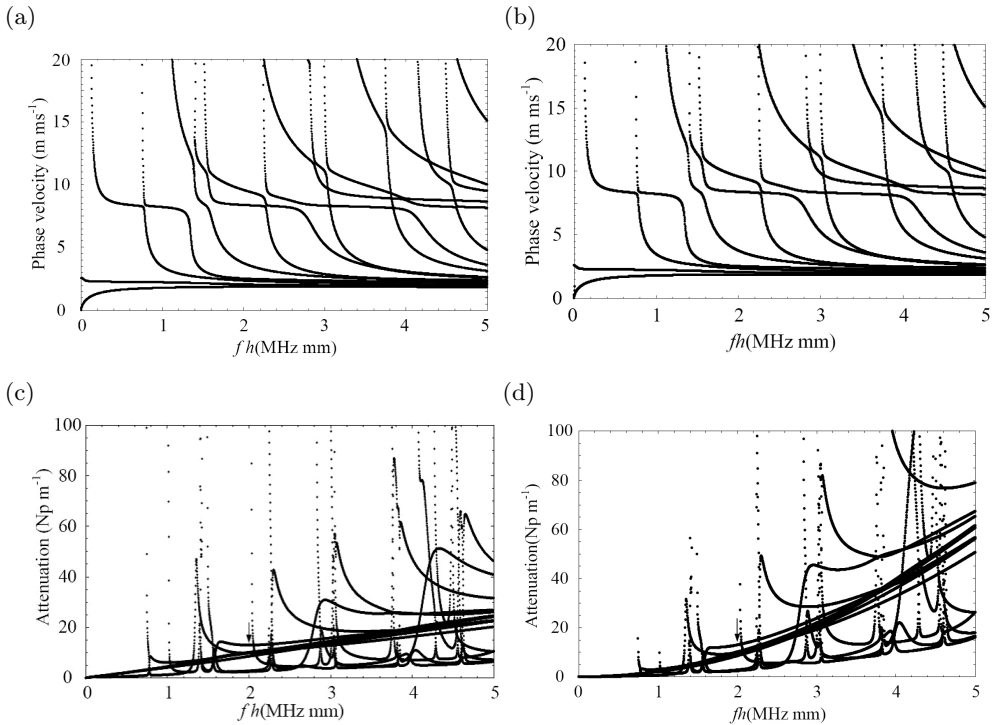


FIG. 7. Attenuation curves for (a) hysteretic model and (c) Kelvin–Voigt model; phase velocity dispersion curves for (b) hysteretic model and (b) Kelvin–Voigt model.

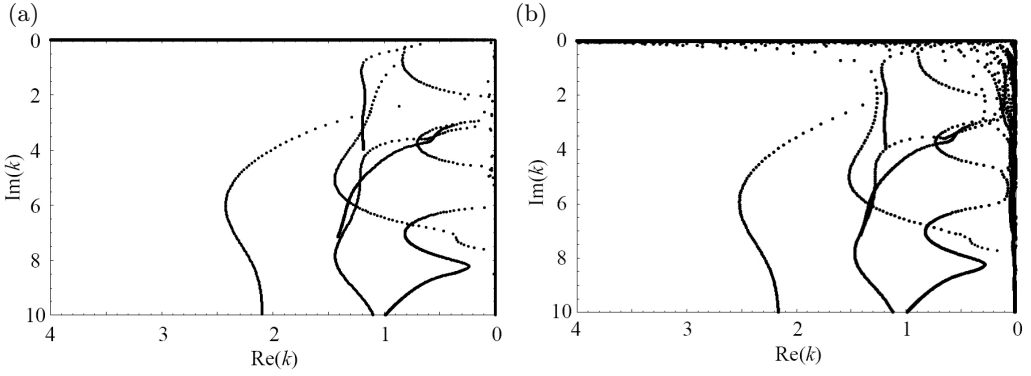


FIG. 8. D top-down view of the 3D spectrum in Fig. 4, in terms of $\text{Re}(k) - \text{Im}(k)$: (a) Kelvin-Voigt model and (b) hysteretic model.

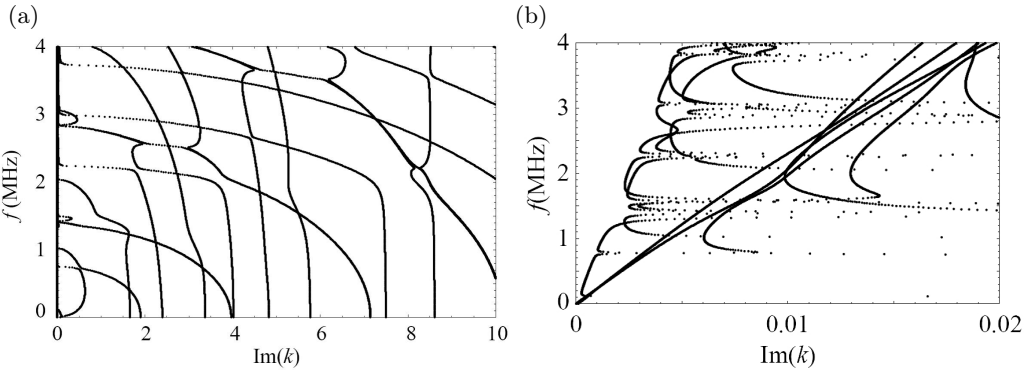


FIG. 9. 2D side-view of the 3D spectrum for the Kelvin-Voigt model; (a) and (b) are the same $f - \text{Im}(k)$ curves using different scales.

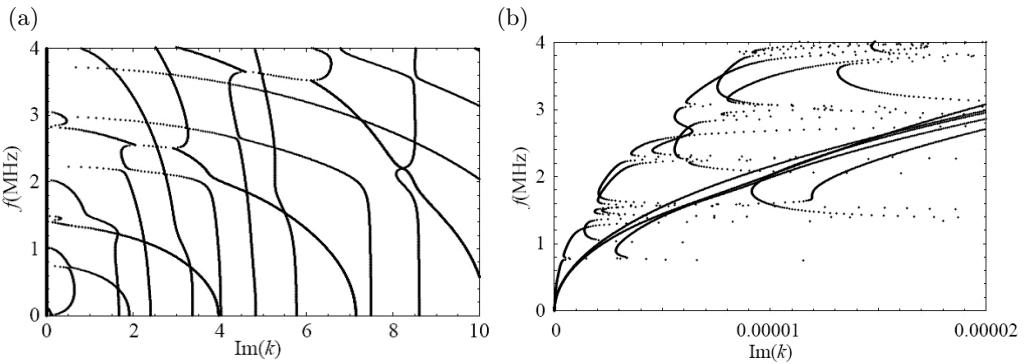


FIG. 10. 2D side-view of the 3D spectrum for the hysteretic model; (a) and (b) are the same $f - \text{Im}(k)$ curves using different scales.

For convenience of contrast, we present the projection view of the 3D spectrum into the $\text{Re}(k)$ – $\text{Im}(k)$ plane for both viscoelastic models, as shown in Fig. 8. Figure 8 indicates the propagating lowly attenuated modes, i.e. with small $\text{Im}(k)$ and large $\text{Re}(k)$, are different for the two models. While for the highly attenuated modes, i.e. with large $\text{Im}(k)$, the $f - \text{Im}(k)$ relations for both viscoelastic models are almost identical, as can be seen in Figs. 9(a) and 10(a). They have distinctions only when $\text{Im}(k)$ is very small, as shown in Figs. 9(b) and 10(b). The reason lies in that the perfectly elastic model already possesses the modes with purely imaginary wavenumbers or complex wavenumbers with large imaginary parts. The variation of such wavenumbers caused by damping is very slight, compared to the existing large $\text{Im}(k)$ in an elastic medium. Instead, for the strongly propagating waves, corresponding to the modes with purely real wavenumbers in the perfectly elastic model, the difference in imaginary wavenumbers for the two viscoelastic models is significant. Such waves can propagate a very long distance and are in effect very useful in non-destructive evaluation.

4.2. Guided circumferential waves in fractional Kelvin–Voigt viscoelastic hollow cylinders

4.2.1. Phase velocity dispersion and attenuation curves. In this section we investigate guided circumferential waves in fractional Kelvin–Voigt viscoelastic hollow cylinders. In order to reveal the influence of fractional order better, we consider the same orthotropic viscoelastic material given in Section 3. The circumferential Lamb-like and SH waves are decoupled, so we treat them separately. Figures 11 and 12 show the phase velocity dispersion and attenuation curves of the integer ($\alpha = 1$) and the fractional order ($\alpha = 0.9$) Kelvin–Voigt viscoelastic hollow cylinders. It can be observed that the fractional order has almost no effects on the phase velocity dispersion but significant effects on the attenuation. The attenuation of the fractional order model is smaller than that of the integer one. For the SH wave, it has a rapid attenuation below the undamped cut-off frequency and reaches a minimum, then almost increases linearly with frequency. The frequency of the minimum attenuation for the fractional order model is slightly smaller than that for the integer one. For the first Lamb-like mode, the attenuation is about linearly increasing from zero frequency. For the higher order modes, the attenuation decreases rapidly from the undamped cut-off frequency and reaches a minimum, then remains almost unchanged (tending to form plateau) in a frequency range in which the phase velocity dispersion curve also has a plateau. After that the attenuation increases first and then decreases and increases in the end with increasing the frequency. For guided wave non-destructive testing of viscoelastic structures, the minimum attenuation frequency is of significance and should be chiefly considered, since it is usually related to the non-dispersive

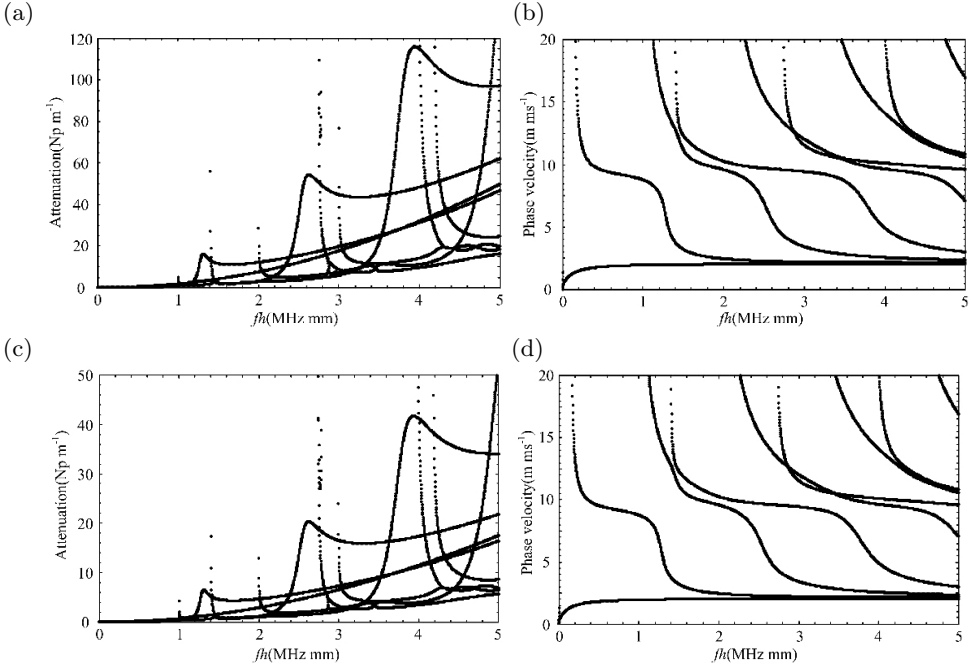


FIG. 11. Lamb-like wave attenuation for (a) the integer model and (c) fractional ($\alpha = 0.9$); phase velocity dispersion for (b) the integer model and (d) fractional ($\alpha = 0.9$) model.

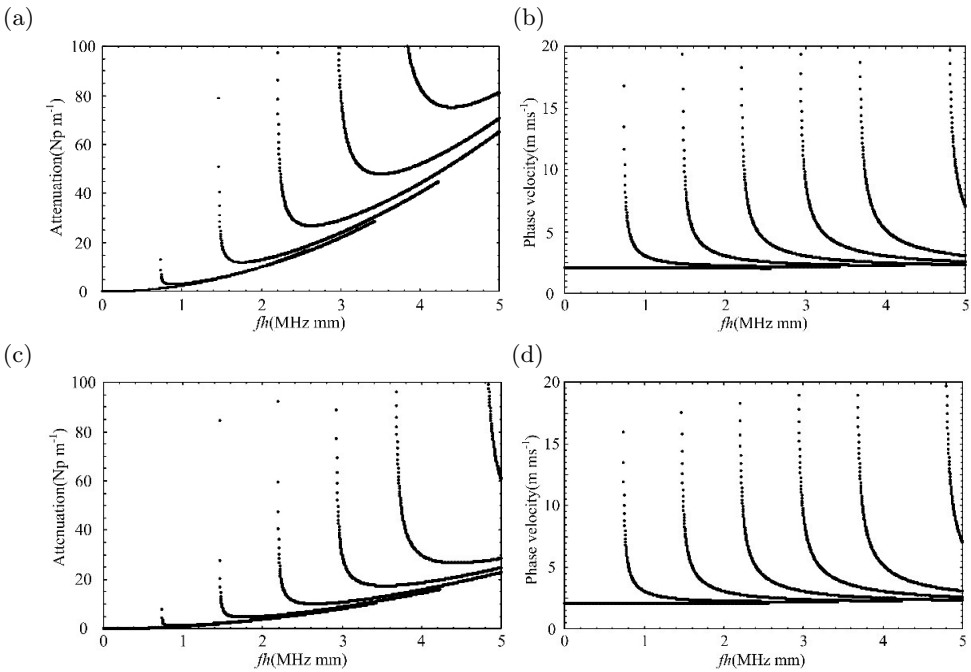


FIG. 12. SH wave attenuation for (a) the integer model and (c) fractional ($\alpha = 0.9$) model; phase velocity dispersion for (b) the integer model and (d) fractional ($\alpha = 0.9$) model.

region. Indeed the great attenuation level is likely associated with strong dispersion of the propagation, which can be illustrated more clearly later when presenting Fig. 15. The attenuation curves show that there are large differences in the attenuation of different modes and this is a major factor in mode selection for practical testing.

4.2.2. Effect of fractional order on phase velocity dispersion and attenuation.

Shown in Fig. 13 there are the attenuation curves of the Lamb-like wave for various fractional Kelvin–Voigt viscoelastic hollow cylinders, with $\alpha = 0.5$, $\alpha = 0.6$ and $\alpha = 0.7$. Comparing Fig. 13(a) to Fig. 13(c), the effect of fractional order is clearly demonstrated. The attenuation becomes smaller as the order decreases. Except for the different attenuation amplitude, the trend of these curves is very similar. For instance, the peak value of the attenuation, for the mode marked A1, reaches 7 Np/m at about 1.3 MHz when $\alpha = 0.7$, and 0.36 Np/m when $\alpha = 0.6$, and 0.12 Np/m when $\alpha = 0.5$. The peak values for the three cases occur at nearly the same frequency. As mentioned above, the fractional order has almost no effect on phase velocity dispersion, so the corresponding phase velocity dispersion curves are not given here.

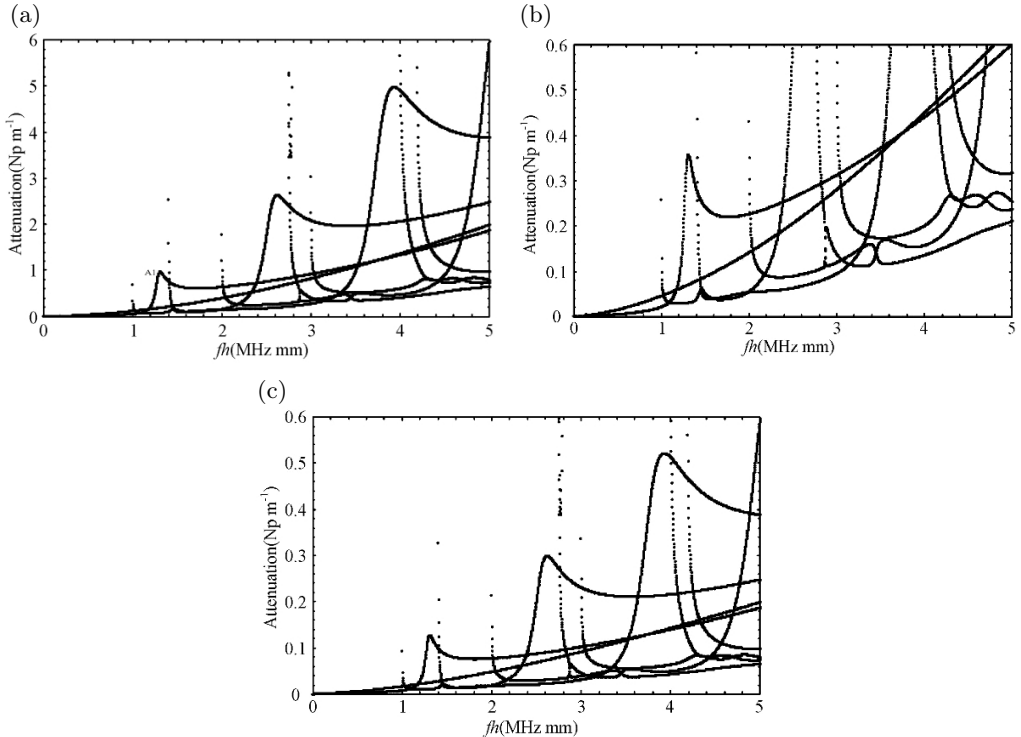


FIG. 13. Attenuation curves for various fractional viscoelastic hollow cylinders, (a) $\alpha = 0.7$, (b) $\alpha = 0.6$, (c) $\alpha = 0.5$.

4.2.3. Effect of material parameters on phase velocity dispersion and attenuation.

The sensitivity of the guided waves to variations of material parameters (C_{ijkl} and μ_{ijkl}) is investigated in this section. To study the effect of the viscoelasticity on phase velocity dispersion and attenuation curves, the viscoelastic rate γ is gradually increased by varying the imaginary parts of the complex moduli from 0.8 to 1.2 [31], of the nominal values given in Section 3. Accordingly Eq. (2.5) becomes:

$$\bar{\bar{C}}_{ijkl} = \tilde{C}_{ijkl} + (-i\omega/\tilde{\omega})^\alpha (\gamma\mu_{ijkl}).$$

Shown in Fig. 14 there are the phase velocity dispersion and attenuation curves for three fractional Kelvin–Voigt viscoelastic hollow cylinders ($\alpha = 0.9$), with $\gamma = 0.8$, $\gamma = 1$ and $\gamma = 1.2$. The nearly identical phase dispersion curve shape in Fig. 14(b) indicates that the effect of changing the imaginary part on the phase velocity dispersion is very little. Contrary on the attenuation curves, as shown in Fig. 14(a), the effect is very strong. The attenuation becomes bigger with the increase of γ , which indicates that the attenuation is related to the viscoelasticity of the hollow cylinder.

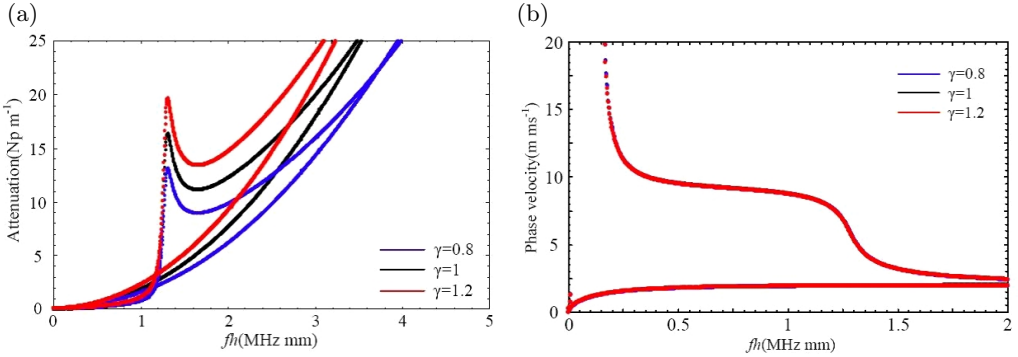


FIG. 14. (a) Attenuation curves and (b) phase velocity dispersion curves for viscoelastic hollow cylinders with different viscoelastic rates.

Similarly, we also calculated the phase velocity dispersion and attenuation curves with variations in the real parts of the complex moduli, namely the elastic moduli. In this case, the complex moduli are set to be

$$\bar{\bar{C}}_{ijkl} = \beta\tilde{C}_{ijkl} + (-i\omega/\tilde{\omega})^\alpha \mu_{ijkl},$$

with, the elastic rate β is varied from 0.8 to 1.2 [31]. Shown in Fig. 15 there are the phase velocity dispersion and attenuation curves for three cases with $\beta = 0.8$, $\beta = 1$ and $\beta = 1.2$. It can be clearly noticed that the effect of changing the real part C_{ij} on both the phase velocity dispersion and attenuation is

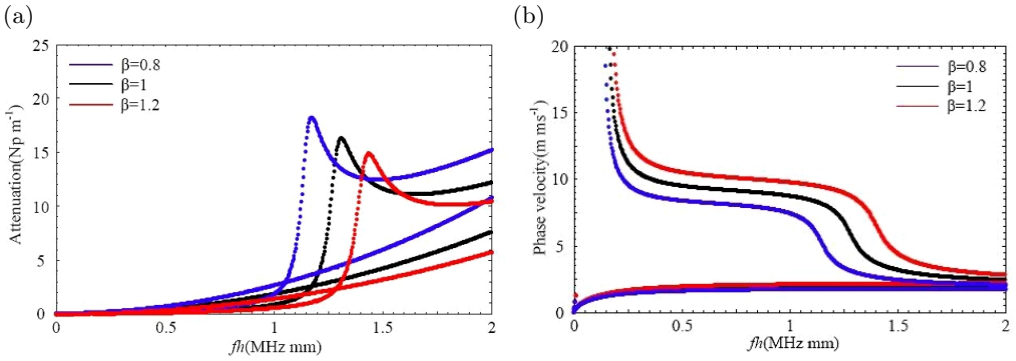


FIG. 15. (a) Attenuation curves and (b) phase velocity dispersion curves for viscoelastic hollow cylinders with different viscoelastic rates.

significant. The greater the elastic rate β , the bigger phase velocity while the smaller the attenuation. This indicates that the phase velocity and attenuation of guided waves are related to the elastic modulus of the viscoelasticity model. Moreover, the non-dispersive region becomes wider with the increase of β , and correspondingly the minimum attenuation frequency range becomes bigger. With the increase of the elastic rate β , the frequency reaching the maximum attenuation increases. The phase velocity dispersion and attenuation curves for the A1 mode with $\beta = 0.8$ are plotted together, as shown in Fig. 16. It is observed that the dispersion becomes strong when the attenuation reaches the maximum, which indicates the great attenuation level is associated with strong dispersion of the propagation. Moreover, the influence of the viscoelastic rate and the elastic rate on the SH wave is similar to that on the Lamb-like wave, so not discussed again here.

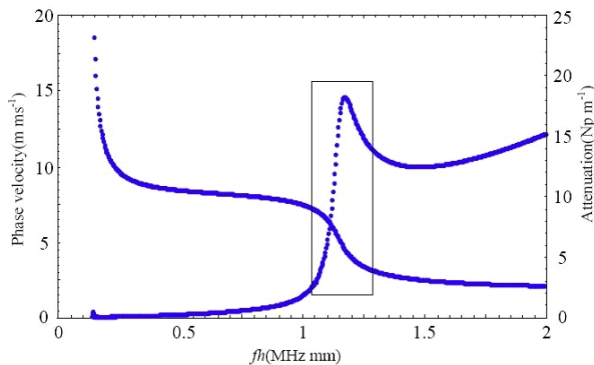


FIG. 16. Phase velocity change of the A1 mode at the frequency of attenuation sudden change.

Further, we investigate the influence of the specified material parameters on phase velocity dispersion and attenuation. Fortunately, the SH wave dispersion relation only involves four parameters besides the material density, i.e. C_{44} , C_{66} , μ_{44} and μ_{66} . We reduce the four parameters to half of the original, and calculate the corresponding phase velocity dispersion and attenuation curves for the fractional order Kelvin–Voigt viscoelastic hollow cylinder with $\alpha = 0.9$, as shown in Figs. 17 and 18. Since the change of μ_{44} and μ_{66} has almost no effect on the phase velocity dispersion, the results are not given here. Figure 17 shows that μ_{44} has a bigger influence on the attenuation curves than μ_{66} , and the influence becomes more significant as the order and frequency increase. The frequency reaching the minimum attenuation value is lower for reducing μ_{44} than that for reducing μ_{66} . Figure 18 shows that the influence of reducing C_{44} is very different from that of reducing C_{66} . When C_{44} is reduced, the overall frequency becomes lower for both the phase velocity dispersion and the attenuation.

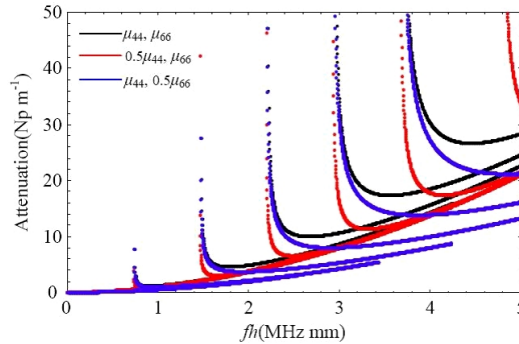


FIG. 17. Attenuation curves for the fractional Kelvin–Voigt viscoelastic hollow cylinder when μ_{44} and μ_{66} are reduced.

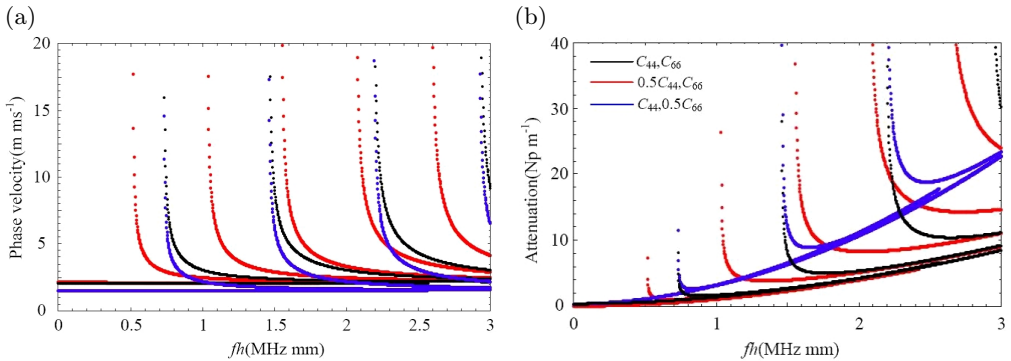


FIG. 18. Phase velocity curves (a) and attenuation curves (b) for the fractional Kelvin–Voigt viscoelastic hollow cylinder when C_{44} and C_{66} are reduced.

has no effect on the phase dispersion of the lowest mode. When C_{66} is reduced, for all modes, the phase velocity becomes smaller but the attenuation becomes larger, in the whole frequency. The minimum attenuation value becomes bigger, contrary to the effect of C_{44} . For higher order modes, C_{66} has very little effect at the early areas of high phase velocity and high attenuation. On the whole, the phase velocity and attenuation mainly is primarily determined by C_{66} and the frequency is chiefly determined by C_{44} .

5. Conclusions

In this study, The Weyl definition of fractional order derivatives and the quadrature-free Legendre polynomial approach are employed to investigate the guided wave in an anisotropic fractional order viscoelastic hollow cylinder. The presented approach transforms the coupled wave differential equations into an eigenvalue problem, avoiding the tedious search procedure by the iterative method. The capability of the presented approach to obtain complete three-dimensional dispersion solutions has been demonstrated, which throws new light onto wave problems involving curved structures or anisotropic viscoelastic media which are often very demanding for conventional approaches. The main results are summarized as follows:

(1) The quadrature-free scheme of the Legendre polynomial approach can dramatically improve the computational efficiency of guided wave problems, which is non-iterative and easy to implement anisotropy is straightforwardly handled and all modes are easily obtained.

(2) For the viscoelastic spectrum, at high frequencies if k satisfies the dispersion relation, then so do $-k$, but not their complex conjugates. This is different from the elastic spectrum.

(3) Both the Kelvin–Voigt and hysteretic viscoelastic models have almost no difference in phase velocity results but have strong influences on attenuation curves. At the low attenuation, the difference of wave features for both viscoelastic models is significant. At the high attenuation, the difference is little.

(4) The fractional order can significantly affect attenuation curves, and the attenuation becomes smaller as the order decreases. The fractional order has almost no effect on phase velocity dispersion. The great attenuation level is likely related to the strong wave dispersion.

(5) The material parameters (elastic modulus and viscoelastic modulus) have significant effects on dispersion and attenuation curves. The viscoelasticity effect on the phase velocity dispersion and attenuation is determined not only by the viscoelastic modulus but also by the elastic modulus. The greater the elastic rate, the bigger phase velocity while the smaller the attenuation.

Appendix

The resulting equations in terms of displacements for an anisotropic fractional Kelvin–Voigt viscoelastic model:

$$\begin{aligned}
 (2.9) \quad & \left\{ r^2 \left(C_{33} \frac{\partial^2 u_r}{\partial r^2} + \eta_{33} \frac{\partial^2}{\partial r^2} \left(\frac{\partial^\alpha u_r}{\partial t^\alpha} \right) + C_{35} \frac{\partial^2 u_\theta}{\partial r^2} + \eta_{35} \frac{\partial^2}{\partial r^2} \left(\frac{\partial^\alpha u_\theta}{\partial t^\alpha} \right) \right. \right. \\
 & + C_{34} \frac{\partial^2 u_z}{\partial r^2} + \eta_{34} \frac{\partial^2}{\partial r^2} \left(\frac{\partial^\alpha u_z}{\partial t^\alpha} \right) + r \left[C_{33} \frac{\partial u_r}{\partial r} + \eta_{33} \frac{\partial}{\partial r} \left(\frac{\partial^\alpha u_r}{\partial t^\alpha} \right) + 2C_{35} \frac{\partial^2 u_r}{\partial r \partial \theta} \right. \\
 & + 2\eta_{35} \frac{\partial^2}{\partial r \partial \theta} \left(\frac{\partial^\alpha u_r}{\partial t^\alpha} \right) + (C_{13} + C_{55}) \frac{\partial^2 u_\theta}{\partial r \partial \theta} + (\eta_{13} + \eta_{55}) \frac{\partial^2}{\partial r \partial \theta} \left(\frac{\partial^\alpha u_\theta}{\partial t^\alpha} \right) - C_{15} \frac{\partial u_\theta}{\partial r} \\
 & - \eta_{15} \frac{\partial}{\partial r} \left(\frac{\partial^\alpha u_\theta}{\partial t^\alpha} \right) + (C_{34} - C_{14}) \frac{\partial u_z}{\partial r} + (\eta_{34} - \eta_{14}) \frac{\partial}{\partial r} \left(\frac{\partial^\alpha u_z}{\partial t^\alpha} \right) \\
 & + (C_{36} + C_{45}) \frac{\partial^2 u_z}{\partial r \partial \theta} + (\eta_{36} + \eta_{45}) \frac{\partial^2}{\partial r \partial \theta} \left(\frac{\partial^\alpha u_z}{\partial t^\alpha} \right) \left. \right] + \left[-C_{11} u_r - \eta_{11} \left(\frac{\partial^\alpha u_r}{\partial t^\alpha} \right) \right. \\
 & + C_{55} \frac{\partial^2 u_r}{\partial \theta^2} + \eta_{55} \frac{\partial^2}{\partial \theta^2} \left(\frac{\partial^\alpha u_r}{\partial t^\alpha} \right) + C_{15} u_\theta + \eta_{15} \left(\frac{\partial^\alpha u_\theta}{\partial t^\alpha} \right) + C_{15} \frac{\partial^2 u_\theta}{\partial \theta^2} + \eta_{15} \frac{\partial^2}{\partial \theta^2} \left(\frac{\partial^\alpha u_\theta}{\partial t^\alpha} \right) \\
 & - (C_{11} + C_{55}) \frac{\partial u_\theta}{\partial \theta} - (\eta_{11} + \eta_{55}) \frac{\partial}{\partial \theta} \left(\frac{\partial^\alpha u_\theta}{\partial t^\alpha} \right) - C_{16} \frac{\partial u_z}{\partial \theta} - \eta_{16} \frac{\partial}{\partial \theta} \left(\frac{\partial^\alpha u_z}{\partial t^\alpha} \right) \\
 & + C_{56} \frac{\partial^2 u_z}{\partial \theta^2} + \eta_{56} \frac{\partial^2}{\partial \theta^2} \left(\frac{\partial^\alpha u_z}{\partial t^\alpha} \right) \left. \right] \pi(r) + \left\{ r^2 \left(C_{33} \frac{\partial u_r}{\partial r} + \eta_{33} \frac{\partial}{\partial r} \left(\frac{\partial^\alpha u_r}{\partial t^\alpha} \right) \right. \right. \\
 & + C_{35} \frac{\partial u_\theta}{\partial r} + \eta_{35} \frac{\partial}{\partial r} \left(\frac{\partial^\alpha u_\theta}{\partial t^\alpha} \right) \left. \right) + r^2 \left(C_{34} \frac{\partial u_z}{\partial r} + \eta_{34} \frac{\partial}{\partial r} \left(\frac{\partial^\alpha u_z}{\partial t^\alpha} \right) \right) \\
 & + r \left[C_{13} u_r + \eta_{13} \left(\frac{\partial^\alpha u_r}{\partial t^\alpha} \right) + C_{35} \frac{\partial u_r}{\partial \theta} + \eta_{35} \frac{\partial}{\partial \theta} \left(\frac{\partial^\alpha u_r}{\partial t^\alpha} \right) - C_{35} u_\theta - \eta_{35} \left(\frac{\partial^\alpha u_\theta}{\partial t^\alpha} \right) \right. \\
 & \left. + C_{13} \frac{\partial u_\theta}{\partial \theta} + \eta_{13} \frac{\partial}{\partial \theta} \left(\frac{\partial^\alpha u_\theta}{\partial t^\alpha} \right) + C_{36} \frac{\partial u_z}{\partial \theta} + \eta_{36} \frac{\partial}{\partial \theta} \left(\frac{\partial^\alpha u_z}{\partial t^\alpha} \right) \right] \left. \right\} \pi'(r) = \rho r^2 \pi(r) \frac{\partial^2 u_r}{\partial t^2},
 \end{aligned}$$

$$\begin{aligned}
 (2.10) \quad & \left\{ r^2 \left(C_{35} \frac{\partial^2 u_r}{\partial r^2} + \eta_{35} \frac{\partial^2}{\partial r^2} \left(\frac{\partial^\alpha u_r}{\partial t^\alpha} \right) + C_{55} \frac{\partial^2 u_\theta}{\partial r^2} + \eta_{55} \frac{\partial^2}{\partial r^2} \left(\frac{\partial^\alpha u_\theta}{\partial t^\alpha} \right) \right. \right. \\
 & + C_{45} \frac{\partial^2 u_z}{\partial r^2} + \eta_{45} \frac{\partial^2}{\partial r^2} \left(\frac{\partial^\alpha u_z}{\partial t^\alpha} \right) \left. \right) + r \left[(C_{15} + 2C_{35}) \frac{\partial u_r}{\partial r} + (\eta_{15} + 2\eta_{35}) \frac{\partial}{\partial r} \left(\frac{\partial^\alpha u_r}{\partial t^\alpha} \right) \right. \\
 & + (C_{13} + C_{55}) \frac{\partial^2 u_r}{\partial r \partial \theta} + (\eta_{13} + \eta_{55}) \frac{\partial^2}{\partial r \partial \theta} \left(\frac{\partial^\alpha u_r}{\partial t^\alpha} \right) + C_{55} \frac{\partial u_\theta}{\partial r} + \eta_{55} \frac{\partial}{\partial r} \left(\frac{\partial^\alpha u_\theta}{\partial t^\alpha} \right) \\
 & \left. + 2C_{15} \frac{\partial^2 u_\theta}{\partial r \partial \theta} + 2\eta_{15} \frac{\partial^2}{\partial r \partial \theta} \left(\frac{\partial^\alpha u_\theta}{\partial t^\alpha} \right) + 2C_{45} \frac{\partial u_z}{\partial r} + 2\eta_{45} \frac{\partial}{\partial r} \left(\frac{\partial^\alpha u_z}{\partial t^\alpha} \right) \right. \\
 & \left. \left. \right] \right\} \pi'(r) = \rho r^2 \pi(r) \frac{\partial^2 u_r}{\partial t^2},
 \end{aligned}$$

$$\begin{aligned}
& + (C_{14} + C_{56}) \frac{\partial^2 u_z}{\partial r \partial \theta} + (\eta_{14} + \eta_{56}) \frac{\partial^2}{\partial r \partial \theta} \left(\frac{\partial^\alpha u_z}{\partial t^\alpha} \right) \Big] + \left[C_{15} \frac{\partial^2 u_r}{\partial \theta^2} + \eta_{15} \frac{\partial^2}{\partial \theta^2} \left(\frac{\partial^\alpha u_r}{\partial t^\alpha} \right) \right. \\
& + (C_{11} + C_{55}) \frac{\partial u_r}{\partial \theta} + (\eta_{11} + \eta_{55}) \frac{\partial}{\partial \theta} \left(\frac{\partial^\alpha u_r}{\partial t^\alpha} \right) + C_{15} u_r + \eta_{15} \left(\frac{\partial^\alpha u_r}{\partial t^\alpha} \right) \\
& + C_{11} \frac{\partial^2 u_\theta}{\partial \theta^2} \eta_{11} \frac{\partial^2}{\partial \theta^2} \left(\frac{\partial^\alpha u_\theta}{\partial t^\alpha} \right) - C_{55} u_\theta - \eta_{55} \left(\frac{\partial^\alpha u_\theta}{\partial t^\alpha} \right) + C_{16} \frac{\partial^2 u_z}{\partial \theta^2} + \eta_{16} \frac{\partial^2}{\partial \theta^2} \left(\frac{\partial^\alpha u_z}{\partial t^\alpha} \right) \\
& + C_{56} \frac{\partial u_z}{\partial \theta} + \eta_{56} \frac{\partial}{\partial \theta} \left(\frac{\partial^\alpha u_z}{\partial t^\alpha} \right) \Big] \pi(r) + \left\{ r^2 (C_{35} \frac{\partial u_r}{\partial r} + \eta_{35} \frac{\partial}{\partial r} \left(\frac{\partial^\alpha u_r}{\partial t^\alpha} \right) + C_{55} \frac{\partial u_\theta}{\partial r} \right. \\
& + \eta_{55} \frac{\partial}{\partial r} \left(\frac{\partial^\alpha u_\theta}{\partial t^\alpha} \right) \Big) + r^2 \left(C_{45} \frac{\partial u_z}{\partial r} + \eta_{45} \frac{\partial}{\partial r} \left(\frac{\partial^\alpha u_z}{\partial t^\alpha} \right) \right) + r \left[C_{15} u_r + \eta_{15} \left(\frac{\partial^\alpha u_r}{\partial t^\alpha} \right) \right. \\
& + C_{55} \frac{\partial u_r}{\partial \theta} + \eta_{55} \frac{\partial}{\partial \theta} \left(\frac{\partial^\alpha u_r}{\partial t^\alpha} \right) - C_{55} u_\theta - \eta_{55} \left(\frac{\partial^\alpha u_\theta}{\partial t^\alpha} \right) + C_{15} \frac{\partial u_\theta}{\partial \theta} \\
& \left. + \eta_{15} \frac{\partial}{\partial \theta} \left(\frac{\partial^\alpha u_\theta}{\partial t^\alpha} \right) + C_{56} \frac{\partial u_z}{\partial \theta} + \eta_{56} \frac{\partial}{\partial \theta} \left(\frac{\partial^\alpha u_z}{\partial t^\alpha} \right) \right] \Big\} \pi'(r) = \rho r^2 \pi(r) \frac{\partial^2 u_\theta}{\partial t^2},
\end{aligned}$$

$$\begin{aligned}
(2.11) \quad & \left\{ r^2 \left(C_{34} \frac{\partial^2 u_r}{\partial r^2} + \eta_{34} \frac{\partial^2}{\partial r^2} \left(\frac{\partial^\alpha u_r}{\partial t^\alpha} \right) + C_{45} \frac{\partial^2 u_\theta}{\partial r^2} + \eta_{45} \frac{\partial^2}{\partial r^2} \left(\frac{\partial^\alpha u_\theta}{\partial t^\alpha} \right) \right. \right. \\
& + C_{44} \frac{\partial^2 u_z}{\partial r^2} + \eta_{44} \frac{\partial^2}{\partial r^2} \left(\frac{\partial^\alpha u_z}{\partial t^\alpha} \right) \Big) + r \left[(C_{14} + C_{34}) \frac{\partial u_r}{\partial r} + (\eta_{14} + \eta_{34}) \frac{\partial}{\partial r} \left(\frac{\partial^\alpha u_r}{\partial t^\alpha} \right) \right. \\
& + (C_{36} + C_{45}) \frac{\partial^2 u_r}{\partial r \partial \theta} + (\eta_{36} + \eta_{45}) \frac{\partial^2}{\partial r \partial \theta} \left(\frac{\partial^\alpha u_r}{\partial t^\alpha} \right) + (C_{14} + C_{56}) \frac{\partial^2 u_\theta}{\partial r \partial \theta} \\
& + (\eta_{14} + \eta_{56}) \frac{\partial^2}{\partial r \partial \theta} \left(\frac{\partial^\alpha u_\theta}{\partial t^\alpha} \right) + C_{44} \frac{\partial u_z}{\partial r} + \eta_{44} \frac{\partial}{\partial r} \left(\frac{\partial^\alpha u_z}{\partial t^\alpha} \right) + 2C_{46} \frac{\partial^2 u_z}{\partial r \partial \theta} \\
& + 2\eta_{46} \frac{\partial^2}{\partial r \partial \theta} \left(\frac{\partial^\alpha u_z}{\partial t^\alpha} \right) \Big] + \left[C_{56} \frac{\partial^2 u_r}{\partial \theta^2} + \eta_{56} \frac{\partial^2}{\partial \theta^2} \left(\frac{\partial^\alpha u_r}{\partial t^\alpha} \right) + C_{16} \frac{\partial u_r}{\partial \theta} + \eta_{16} \frac{\partial}{\partial \theta} \left(\frac{\partial^\alpha u_r}{\partial t^\alpha} \right) \right. \\
& + C_{16} \frac{\partial^2 u_\theta}{\partial \theta^2} + \eta_{16} \frac{\partial^2}{\partial \theta^2} \left(\frac{\partial^\alpha u_\theta}{\partial t^\alpha} \right) - C_{56} \frac{\partial u_\theta}{\partial \theta} - \eta_{56} \frac{\partial}{\partial \theta} \left(\frac{\partial^\alpha u_\theta}{\partial t^\alpha} \right) + C_{66} \frac{\partial^2 u_z}{\partial \theta^2} \\
& + \eta_{66} \frac{\partial^2}{\partial \theta^2} \left(\frac{\partial^\alpha u_z}{\partial t^\alpha} \right) \Big] \pi(r) \Big\} + \left\{ r^2 (C_{34} \frac{\partial u_r}{\partial r} + \eta_{34} \frac{\partial}{\partial r} \left(\frac{\partial^\alpha u_r}{\partial t^\alpha} \right) + C_{45} \frac{\partial u_\theta}{\partial r} \right. \\
& + \eta_{45} \frac{\partial}{\partial r} \left(\frac{\partial^\alpha u_\theta}{\partial t^\alpha} \right) \Big) + r^2 \left(C_{44} \frac{\partial u_z}{\partial r} + \eta_{44} \frac{\partial}{\partial r} \left(\frac{\partial^\alpha u_z}{\partial t^\alpha} \right) \right) + r \left[C_{14} u_r + \eta_{14} \left(\frac{\partial^\alpha u_r}{\partial t^\alpha} \right) \right. \\
& + C_{45} \frac{\partial u_r}{\partial \theta} + \eta_{45} \frac{\partial}{\partial \theta} \left(\frac{\partial^\alpha u_r}{\partial t^\alpha} \right) - C_{45} u_\theta - \eta_{45} \left(\frac{\partial^\alpha u_\theta}{\partial t^\alpha} \right) + C_{14} \frac{\partial u_\theta}{\partial \theta} + \eta_{14} \frac{\partial}{\partial \theta} \left(\frac{\partial^\alpha u_\theta}{\partial t^\alpha} \right) \\
& \left. + C_{46} \frac{\partial u_z}{\partial \theta} + \eta_{46} \frac{\partial}{\partial \theta} \left(\frac{\partial^\alpha u_z}{\partial t^\alpha} \right) \right] \Big\} \pi'(r) = \rho r^2 \pi(r) \frac{\partial^2 u_z}{\partial t^2}.
\end{aligned}$$

For the orthotropic case, Eqs. (2.9), (2.10) and (2.11) are simplified to:

$$\begin{aligned}
 (2.12) \quad & \left\{ r^2 \left(C_{33} \frac{\partial^2 u_r}{\partial r^2} + \eta_{33} \frac{\partial^2}{\partial r^2} \left(\frac{\partial^\alpha u_r}{\partial t^\alpha} \right) \right) + r \left[C_{33} \frac{\partial u_r}{\partial r} + \eta_{33} \frac{\partial}{\partial r} \left(\frac{\partial^\alpha u_r}{\partial t^\alpha} \right) \right. \right. \\
 & + (C_{13} + C_{55}) \frac{\partial^2 u_\theta}{\partial r \partial \theta} + (\eta_{13} + \eta_{55}) \frac{\partial^2}{\partial r \partial \theta} \left(\frac{\partial^\alpha u_\theta}{\partial t^\alpha} \right) \left. \left. + \left[-C_{11} u_r - \eta_{11} \left(\frac{\partial^\alpha u_r}{\partial t^\alpha} \right) \right. \right. \right. \\
 & + C_{55} \frac{\partial^2 u_r}{\partial \theta^2} + \eta_{55} \frac{\partial^2}{\partial \theta^2} \left(\frac{\partial^\alpha u_r}{\partial t^\alpha} \right) - (C_{11} + C_{55}) \frac{\partial u_\theta}{\partial \theta} - (\eta_{11} + \eta_{55}) \frac{\partial}{\partial \theta} \left(\frac{\partial^\alpha u_\theta}{\partial t^\alpha} \right) \left. \left. \right] \right\} \pi(r) \\
 & + \left\{ r^2 \left(C_{33} \frac{\partial u_r}{\partial r} + \eta_{33} \frac{\partial}{\partial r} \left(\frac{\partial^\alpha u_r}{\partial t^\alpha} \right) \right) + r \left[C_{13} u_r + \eta_{13} \left(\frac{\partial^\alpha u_r}{\partial t^\alpha} \right) + C_{13} \frac{\partial u_\theta}{\partial \theta} \right. \right. \\
 & \left. \left. + \eta_{13} \frac{\partial}{\partial \theta} \left(\frac{\partial^\alpha u_\theta}{\partial t^\alpha} \right) \right] \right\} \pi'(r) = \rho r^2 \pi(r) \frac{\partial^2 u_r}{\partial t^2},
 \end{aligned}$$

$$\begin{aligned}
 (2.13) \quad & \left\{ r^2 (C_{55} \frac{\partial^2 u_\theta}{\partial r^2} + \eta_{55} \frac{\partial^2}{\partial r^2} \left(\frac{\partial^\alpha u_\theta}{\partial t^\alpha} \right)) + r \left[(C_{13} + C_{55}) \frac{\partial^2 u_r}{\partial r \partial \theta} \right. \right. \\
 & + (\eta_{13} + \eta_{55}) \frac{\partial^2}{\partial r \partial \theta} \left(\frac{\partial^\alpha u_r}{\partial t^\alpha} \right) + C_{55} \frac{\partial u_\theta}{\partial r} + \eta_{55} \frac{\partial}{\partial r} \left(\frac{\partial^\alpha u_\theta}{\partial t^\alpha} \right) \left. \right] \\
 & + \left[(C_{11} + C_{55}) \frac{\partial u_r}{\partial \theta} + (\eta_{11} + \eta_{55}) \frac{\partial}{\partial \theta} \left(\frac{\partial^\alpha u_r}{\partial t^\alpha} \right) + C_{11} \frac{\partial^2 u_\theta}{\partial \theta^2} + \eta_{11} \frac{\partial^2}{\partial \theta^2} \left(\frac{\partial^\alpha u_\theta}{\partial t^\alpha} \right) \right. \\
 & \left. - C_{55} u_\theta - \eta_{55} \left(\frac{\partial^\alpha u_\theta}{\partial t^\alpha} \right) \right] \right\} \pi(r) + \left\{ r^2 (C_{55} \frac{\partial u_\theta}{\partial r} + \eta_{55} \frac{\partial}{\partial r} \left(\frac{\partial^\alpha u_\theta}{\partial t^\alpha} \right)) \right. \\
 & \left. + r \left[C_{55} \frac{\partial u_r}{\partial \theta} + \eta_{55} \frac{\partial}{\partial \theta} \left(\frac{\partial^\alpha u_r}{\partial t^\alpha} \right) - C_{55} u_\theta - \eta_{55} \left(\frac{\partial^\alpha u_\theta}{\partial t^\alpha} \right) \right] \right\} \pi'(r) = \rho r^2 \pi(r) \frac{\partial^2 u_\theta}{\partial t^2},
 \end{aligned}$$

$$\begin{aligned}
 (2.14) \quad & \left\{ r^2 (C_{44} \frac{\partial^2 u_z}{\partial r^2} + \eta_{44} \frac{\partial^2}{\partial r^2} \left(\frac{\partial^\alpha u_z}{\partial t^\alpha} \right)) + r \left[C_{44} \frac{\partial u_z}{\partial r} + \eta_{44} \frac{\partial}{\partial r} \left(\frac{\partial^\alpha u_z}{\partial t^\alpha} \right) \right] \right. \\
 & \left. + \left[C_{66} \frac{\partial^2 u_z}{\partial \theta^2} + \eta_{66} \frac{\partial^2}{\partial \theta^2} \left(\frac{\partial^\alpha u_z}{\partial t^\alpha} \right) \right] \right\} \pi(r) + r^2 \left(C_{44} \frac{\partial u_z}{\partial r} + \eta_{44} \frac{\partial}{\partial r} \left(\frac{\partial^\alpha u_z}{\partial t^\alpha} \right) \right) \pi'(r) \\
 & = \rho r^2 \pi(r) \frac{\partial^2 u_z}{\partial t^2}.
 \end{aligned}$$

The matrix elements in Eq. (17) are:

$$A_{11}^{j,m} = -b^2 (C_{55} + (-i\omega)^\alpha \eta_{55}) u(m, 0, 0, j),$$

$$A_{22}^{j,m} = -b^2 (C_{11} + (-i\omega)^\alpha \eta_{11}) u(m, 0, 0, j),$$

$$A_{33}^{j,m} = -b^2 (C_{66} + (-i\omega)^\alpha \eta_{66}) u(m, 0, 0, j),$$

$$A_{12}^{j,m} = A_{21}^{j,m} = A_{13}^{j,m} = A_{31}^{j,m} = A_{23}^{j,m} = A_{32}^{j,m} = 0;$$

$$\begin{aligned}
B_{12}^{j,m} &= \{ib(C_{13} + (-i\omega)^\alpha \eta_{13} + C_{55} + (-i\omega)^\alpha \eta_{55})u(m, 1, 1, j) \\
&\quad - ib(C_{11} + (-i\omega)^\alpha \eta_{11})u(m, 0, 0, j) \\
&\quad - ib(C_{55} + (-i\omega)^\alpha \eta_{55})u(m, 0, 0, j) + ib(C_{13} + (-i\omega)^\alpha \eta_{13})k(m, 1, 0, j)\}, \\
B_{21}^{j,m} &= \{ib(C_{13} + (-i\omega)^\alpha \eta_{13} + C_{55} + (-i\omega)^\alpha \eta_{55})u(m, 1, 1, j) \\
&\quad + ibC_{55}u(m, 0, 0, j) + ib(-i\omega)^\alpha \eta_{55}u(m, 0, 0, j) \\
&\quad + ib(C_{11} + (-i\omega)^\alpha \eta_{11})u(m, 0, 0, j) + ib(C_{55} + (-i\omega)^\alpha \eta_{55})k(m, 1, 0, j)\}, \\
B_{11}^{j,m} &= B_{22}^{j,m} = B_{33}^{j,m} = B_{13}^{j,m} = B_{31}^{j,m} = B_{23}^{j,m} = B_{32}^{j,m} = 0; \\
C_{11}^{j,m} &= \{(C_{33} + (-i\omega)^\alpha \eta_{33})u(m, 2, 2, j) + (C_{33} + (-i\omega)^\alpha \eta_{33})u(m, 1, 1, j) \\
&\quad - (C_{11} + (-i\omega)^\alpha \eta_{11})u(m, 0, 0, j) + (C_{33} + (-i\omega)^\alpha \eta_{33})k(m, 2, 1, j) \\
&\quad + (C_{13} + (-i\omega)^\alpha \eta_{13})k(m, 1, 0, j)\}, \\
C_{22}^{j,m} &= \{(C_{55} + (-i\omega)^\alpha \eta_{55})u(m, 2, 2, j) + (C_{55} + (-i\omega)^\alpha \eta_{55})u(m, 1, 1, j) \\
&\quad - (C_{55} + (-i\omega)^\alpha \eta_{55})u(m, 0, 0, j) + (C_{55} + (-i\omega)^\alpha \eta_{55})k(m, 2, 1, j) \\
&\quad - (C_{55} + (-i\omega)^\alpha \eta_{55})k(m, 1, 0, j)\}, \\
C_{33}^{j,m} &= \{(C_{44} + (-i\omega)^\alpha \eta_{44})u(m, 2, 2, j) + (C_{44} + (-i\omega)^\alpha \eta_{44})u(m, 1, 1, j) \\
&\quad + (C_{44} + (-i\omega)^\alpha \eta_{44})k(m, 2, 1, j)\}, \\
C_{12}^{j,m} &= C_{21}^{j,m} = C_{13}^{j,m} = C_{31}^{j,m} = C_{23}^{j,m} = C_{32}^{j,m} = 0; \\
M_m^j &= \rho u(m, 2, 0, j),
\end{aligned}$$

where

$$\begin{aligned}
u(m, l, n, j) &= \int_a^b Q_j^*(r) r^l \frac{\partial^n Q_m(r)}{\partial r^n} dr; \\
k(m, l, n, j) &= \int_a^b Q_j^*(r) r^l \frac{\partial \pi(r)}{\partial r} \frac{\partial^n Q_m(r)}{\partial r^n} dr.
\end{aligned}$$

Disclosure statement

No potential conflict of interest was reported by the author.

Acknowledgements

The work was supported by the National Natural Science Foundation of China (No. 51975189 and U1804134), the Training Plan of Young Key Teachers of Universities in Henan Province (No.2018-GGJS-060), and the open fund project of Henan Key Laboratory of underground engineering and disaster prevention and control.

References

1. I. BARTOLI, A. MARZANI, H. MATT, F.L.D. SCALEA, E. VIOLA, *Modeling wave propagation in damped waveguides of arbitrary cross-section*, Journal of Sound and Vibration, **295**, 685–707, 2006.
2. T. HAYASHI, W.J. SONG, J.L. ROSE, *Guided wave dispersion curves for a bar with an arbitrary cross-section, a rod and rail example*, Ultrasonics, **41**, 3, 175–183, 2003.
3. A. KARMAZIN, E. KIRILLOVA, W. SEEMANN, P. SYROMYATNIKOV, *Investigation of Lamb elastic waves in anisotropic multilayered composites applying the Green's matrix*, Ultrasonics, **51**, 1, 17–28, 2011.
4. S.I. ROKHLIN, L. WANG, *Stable recursive algorithm for elastic wave propagation in layered anisotropic media: stiffness matrix method*, Journal of the Acoustical Society of America, **112**, 822–834, 2002.
5. X. ZHANG, Z. LI, X. WANG, J. YU, *The fractional Kelvin–Voigt model for circumferential guided waves in a viscoelastic FGM hollow cylinder*, Applied Mathematical Modelling, **89**, 299–313, 2021.
6. S.V. KUZNETSOV, *Lamb waves in stratified and functionally graded plates: discrepancy, similarity, and convergence*, Wave Random Complex, 1683257, 1–10, 2019.
7. F. SIMONETTI, M.J.S. LOWE, *On the meaning of Lamb mode nonpropagating branches*, Journal of the Acoustical Society of America, **118**, 1, 186–192, 2005.
8. F. ZHU, B. WANG, Z. QIAN, E. PAN, *Accurate characterization of 3D dispersion curves and mode shapes of waves propagating in generally anisotropic viscoelastic/elastic plates*, International Journal of Solids and Structures, **150**, 52–65, 2018.
9. B. PAVLAKOVIC, M. LOWE, *Disperse User's Manual Version 2.0*, Imperial College, University of London, London, 2001.
10. M. ZHENG, C. HE, Y. LYU, B. WU, *Guided waves propagation in anisotropic hollow cylinders by Legendre polynomial solution based on state-vector formalism*, Composite Structures, **207**, 645–657, 2019.
11. M. CASTAINGS, B. HOSTEN, *Guided waves propagating in sandwich structures made of anisotropic, viscoelastic, composite materials*, Journal of the Acoustical Society of America, **113**, 2622–2634, 2003.
12. B. HOSTEN, M. CASTAINGS, *Transfer matrix of multilayered absorbing and anisotropic media. Measurements and simulations of ultrasonic wave propagation through composite materials*, Journal of the Acoustical Society of America, **94**, 1488–1495, 1993.
13. M.A. TORRES-ARREDONDO, C.P. FRITZEN, *A viscoelastic plate theory for the fast modelling of Lamb wave solutions in NDT/SHM applications*, Ultrasound, **66**, 7–13, 2011.
14. C. OTHMANI, S. DAHMEN, A. NJEH, M.H.B. GHOZLEN, *Investigation of guided waves propagation in orthotropic viscoelastic carbon–epoxy plate by Legendre polynomial method*, Mechanics Research Communications, **74**, 27–33, 2016.
15. J.G. YU, *Viscoelastic shear horizontal wave in graded and layered plates*, International Journal of Solids and Structures, **48**, 2361–2372, 2011.
16. S. DAHMEN, M.B. AMOR, M.H.B. GHOZLEN, *Investigation of the coupled Lamb waves propagation in viscoelastic and anisotropic multilayer composites by Legendre polynomial method*, Composite Structures, **153**, 557–568, 2016.

17. H. CUNFU, L. HONGYE, L. ZENGHUA, W. BIN, *The propagation of coupled Lamb waves in multilayered arbitrary anisotropic composite laminates*, Journal of Sound and Vibration, **332**, 7243–7256, 2013.
18. E. MANCONI, B.R. MACE, R. GARZIERA, *The loss-factor of pre-stressed laminated curved panels and cylinders using a wave and finite element method*, Journal of Sound and Vibration, **332**, 1704–1711, 2013.
19. F.H. QUINTANILLA, M.J.S. LOWE, R.V. CRASTER, *Full 3D dispersion curve solutions for guided waves in generally anisotropic media*, Journal of Sound and Vibration, **363**, 545–559, 2016.
20. F.H. QUINTANILLA, Z. FAN, M.J.S. LOWE, R.V. CRASTER, *Guided waves' dispersion curves in anisotropic viscoelastic single-and multi-layered media*, Proceedings of the Royal Society A: Mathematical, Physical and Engineering Sciences, **471**, 20150268, 2015.
21. M.S. CHAKI, A.K. SINGH, *Anti-plane wave in a piezoelectric viscoelastic composite medium: a semi-analytical finite element approach using PML*, International Journal of Applied Mechanics, **12**, 2050020, 2020.
22. M. MAZZOTTI, A. MARZANI, I. BARTOLI, E VIOLA, *Guided waves dispersion analysis for prestressed viscoelastic waveguides by means of the SAFE method*, International Journal of Solids and Structures, **49**, 2359–2372, 2012.
23. D. REN, X. SHEN, C. LI, X. CAO, *The fractional Kelvin–Voigt model for Rayleigh surface waves in viscoelastic FGM infinite half space*, Mechanics Research Communications, **87**, 53–58, 2017.
24. R.C. KOELLER, *Applications of fractional calculus to the theory of viscoelasticity*, Journal of Applied Mechanics, **51**, 299–307, 1984.
25. M.D. PAOLA, A. PIRROTTA, A. VALENZA, *Visco-elastic behavior through fractional calculus: an easier method for best fitting experimental results*, Mechanics of Materials, **43**, 799–806, 2011.
26. L.B. ELDRDRED, W.P. BAKER, A.N. PALAZOTTO, *Kelvin–Voigt versus fractional derivative model as constitutive relations for viscoelastic materials*, AIAA Journal, **33**, 3, 547–550, 1995.
27. B. WU, Y. SU, D. LIU, W. CHEN., C. ZHANG, *On propagation of axisymmetric waves in pressurized functionally graded elastomeric hollow cylinders*, Journal of Sound and Vibration, **421**, 17–47, 2018.
28. A. SAFARI-KAHNAKI, S.M. HOSSEINI, M. TAHANI, *Thermal shock analysis and thermo-elastic stress waves in functionally graded thick hollow cylinders using analytical method*, International Journal of Mechanics and Materials in Design, **7**, 3, 167–184, 2011.
29. C. BARON, *Propagation of elastic waves in an anisotropic functionally graded hollow cylinder in vacuum*, Ultrasonics, **51**, 2, 123–130, 2011.
30. G. NEAU, *Lamb Waves in Anisotropic Viscoelastic Plates. Study of the Wave Fronts and Attenuation*, PhD Thesis, University Bordeaux I, Bordeaux, 2003.
31. H.X. SUN, B.Q. XU, H. ZHANG, Q. GAO, S.Y. ZHANG, *Influence of adhesive layer properties on laser-generated ultrasonic waves in thin bonded plates*, Chinese Physics B, **20**, 014302, 2011.

32. M. DERAKHSHAN, A. AMINATAEI, *An iterative method for solving fractional diffusion-wave equation involving the Caputo–Weyl fractional derivative*, Numerical Linear Algebra, e2345, 2020.
33. G. FAILLA, M. ZINGALES, *Advanced materials modelling via fractional calculus: challenges and perspectives*, Philosophical Transactions of the Royal Society A, **378**, 20200050, 2020.
34. T.J. BRIDGES, P.J. MORRIS, *Differential eigenvalue problems in which the parameter appears nonlinearly*, Journal of Computational Physics, **55**, 437–460, 1984.

Received August 23, 2020; revised version December 17, 2020.

Published online March 31, 2021.
